Circuits and Systems
Mekelweg 4,
2628 CD Delft
The Netherlands
http://ens.ewi.tudelft.nl/

CAS-2020-00

M.Sc. Thesis

Two-Dimensional Blood Flow Estimation in the Brain with Ultrafast Ultrasound

Karishma Kumar

Abstract

Detailed imaging of blood flow may improve the understanding of brain functions. The state-of-the-art non-invasive flow imaging of the brain is limited to a one-dimensional Doppler setting. We propose a method to estimate the two-dimensional flow vector in the fine vascular network of the brain by using a speckle tracking technique. The framework of Orthogonal Matching Pursuit is used for speckle tracking and modified to include prior constraints to guide the matching process among two frames, called as Guided Orthogonal Matching Pursuit. Prior constraint is in the form of a directional constraint which determines the probability of vector flow in all the directions according to the orientation of the vessels. The orientation of the vessels is computed using Power Doppler Imaging. In this work, the proposed method for two-dimensional vector estimation is compared with the standard block matching technique of Normalized Cross-Correlation. We see that the variance of the final velocity estimates has reduced when compared to the standard speckle tracking method and the direction of blood flow is found within the curvature of the vessel.

Two-Dimensional Blood Flow Estimation in the Brain with Ultrafast Ultrasound

Thesis

submitted in partial fulfillment of the
requirements for the degree of

Master of Science

in

Signals and Systems

by

Karishma Kumar
born in Chandigarh, India

This work was performed in:

Circuits and Systems Group
Department of Electrical Engineering
Faculty of Electrical Engineering, Mathematics and Computer Science
Delft University of Technology

Delft University of Technology

Delft University of Technology
Department of
Electrical Engineering

The undersigned hereby certify that they have read and recommend to the Faculty of Electrical Engineering, Mathematics and Computer Science for acceptance a thesis entitled **"Two-Dimensional Blood Flow Estimation in the Brain with Ultrafast Ultrasound"** by **Karishma Kumar** in partial fulfillment of the requirements for the degree of **Master of Science**.

Dated: 22-01-2020

Chairman: _____
prof.dr.ir. G. Leus

Advisor: _____
dr.ir. P.Kruizinga

Committee Members: _____
dr.ir. M.A.P. Pertijs

_____
ir. B.S. Generowicz

Acknowledgments

I would like to thank my advisor dr.ir. P.Kruizinga for his constant guidance and support during the entire duration of my thesis and also to the entire CUBE team at Erasmus Medical Centre, who kept me motivated with their dedication to improve and develop the ultrasound scanning modality.

I would like to thank my supervisor at TU Delft, prof.dr.ir. G. Leus who was available every time I needed help and provided me with the required ideas to tackle the problems at hand. I am grateful to all my friends from TU Delft with whom it was possible to run this marathon lasting for about a year.

The implementation of my work would haven been really challenging without the help of Jason Voorneveld, who is a Postdoctral researcher at Erasmus MC. I am grateful to Jason for letting me use his work that led me to the completion of my own work. I would like to thank my daily supervisor at Erasmus MC, Bas Generowicz to whom I went directly when there were issues related to my thesis for which he always had legal hacks.

My thesis journey has taught me valuable lessons. Among its many lessons, one of it is to keep on trying without worrying about the consequences. I connected with this lesson deeply in the later stages of my thesis where I was more productive as I started to embrace my mistakes little by little and effectively learn by making them. This thought process was transferred from the mindset that I developed while doing challenging workouts with Spartans. I am thankful to all my friends in that workout and would like to specially thank Bart van de Laar, who is the lead instructor for the Spartan workout, for introducing me to such an environment.

I am obliged to mention my friends who tried to counsel me for various things. I want to thank Pranav, Manoj, Bishwadeep, Yuan, Aravind, Mado, Rene and Aybuke for being there for me.

Master of Science would have not been possible without my family's support and guidance in the first place. I am thankful to all the members of my family who are there with me at each and almost every step of my life.

Karishma Kumar
Delft, The Netherlands
22-01-2020

Contents

Abbreviations

CNR Contrast-to-Noise ratio

GOMP Guided Orthogonal Matching Pursuit

MD Mean Deviation

MSE Mean Square Error

NCC Normalized Cross-Correlation

OMP Orthogonal Matching Pursuit

PCC Pearson Correlation Coefficient

PDI Power Doppler Image

PIT Pulse Interval Time

PRF Pulse Repetition Frequency

PSD Power Spectral Density

RBC Red Blood Cells

SNR Signal-to-Noise ratio

Nomenclature

$\hat{CF_b}$	Fourier Transform of CF_b in slow-time
λ_0	Wavelength of ultrasonic plane waves
ω_s	Angular frequency of slow-time
$\mathbf{b}$	Selection vector in system model
$\mathbf{D}$	Dictionary matrix of shifted blocks in system model
$\mathbf{r}$	Residue vector used in matching pursuit
$\mathbf{y}$	Vectorized pixels of a block in system model
θ_v	Vessel orientation in degrees
BF	Beamformed frame
BF_H	Hilbert transformed beamformed frame
c	Speed of sound in the scanning region
CF	Compounded frame
CF_b	Filtered compounded frame
$d_m(z,x)$	Distance between m^{th} element and the spatial position (z,x) in the scanning region
f_0	Central frequency of ultrasonic plane waves
j	Sequence repetition index
m	Element index in a transducer array
n	Angle increment index
N_{angles}	Total number of emitted plane waves in a sequence
n_{avg}	Number of filtered frame pairs averaged to provide frame-wise estimates
$N_{ensemble}$	Total number of frames averaged to compute a Power Doppler Image
s_m	Backscattered echoes recorded by the m^{th} element
t_{fm}	time taken by the plane wave to reach the m^{th} element (referred to as *fast-time*)
T_{frame}	Total time take to scan one frame
t_s	Acquisition time for a emitted plane wave frame (referred to as *slow-time*)
v_d	Velocity of the scatterers measured by the Doppler method
w	Spatial weight
x	Spatial position in the lateral direction
z	Spatial position in the axial

1 Introduction

Ultrasound Imaging is a non-invasive method which is frequently used in medical diagnosis. Blood flow imaging techniques have been vastly investigated for focused ultrasound emission [1]. Parallel emission systems have drawn attention in recent years as they provide faster scanning times.

In the brain imaging sector, extensive research has been carried out to understand the brain using MRI [2] tools. A new focus has emerged to scan the brain through the use of ultrasonic waves. This emergence of interest is due to the high potential that ultrasound offers in terms of speed of operation, lower costs and the resulting high spatial-temporal resolution [3]. The high frame rate of unfocused parallel beams comes with its demerits. The received response of a plane wave emission suffers from a loss of spatial awareness which arises when the whole region is scanned at once. At the time of reception, the transducer elements receive a signal from the whole region of interest which causes a reduction in the spatial resolution. Therefore the scan suffers from a low Signal-to-Noise ratio (SNR) and a Contrast-to-Noise ratio (CNR). [3].

To increase the SNR and CNR values, plane waves are emitted not just once but at multiple times at different firing angles and then coherently added together to form a compound image. This sequence of emission of plane waves is termed as *ultrafast ultrasound*. [3].

As the name suggests, this newer method is faster than the conventional line-by-line scanning method as illustrated in Figure 1.1.

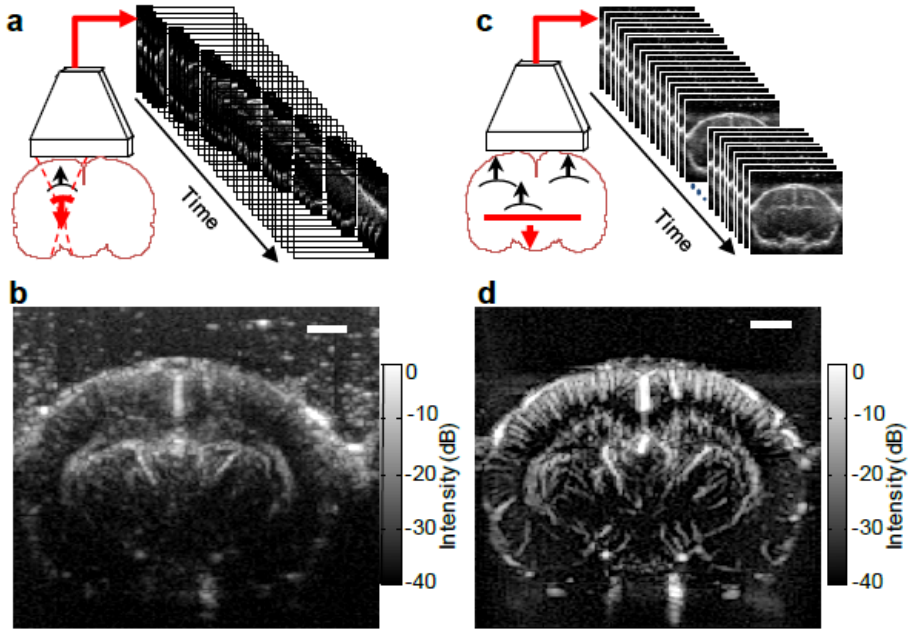

Figure 1.1: Comparison between the line-by-line conventional ultrasound (a, b) and the ultrafast ultrasound (c, d). The data acquisition steps are shown in the upper half and the final Power Doppler images for the same scanning time are shown in the lower half. Clearly, the image quality using the ultrafast method is the best of the two. Figure is adopted from [4].

Problem Definition

The current state-of-the-art imaging of blood flow estimation in the brain showcases blood velocities which have flow mainly in the direction of the emitted ultrasonic plane waves. The flow information is obtained for one dimension using the Ultrafast Ultrasound [4]. The objective of this thesis is to investigate blood flow in all directions of the two-dimensional scanning region using the Ultrafast Ultrasound. The proposed method aims at producing reliable velocity estimates of blood flow in the brain by guiding the velocity estimates of speckle tracking with prior information obtained by Power Doppler Imaging.

Thesis Outline

In Section 1.1, an overall view of our system from the earliest step of data acquisition by the elements of the transducer array until the estimation of the velocity flow is explained. The following Section 1.2 presents the current state-of-the-art techniques used to estimate the blood flow in the brain. Issues with the current imaging methods are laid out in Section 1.3.

The general flow visualization techniques for ultrasound are explained and illustrated in Chapter 2, after which Chapter 3 focuses on the proposed methodology of the Guided Orthogonal Matching Pursuit (GOMP) for velocity estimation in the brain. To

implement GOMP, prior knowledge regarding the orientation of the vessels is required. A method is developed and explained in Chapter 3 to find the orientation of the fine vascular network of the brain. The k-Wave toolbox is used to produce the simulation data-set. The setup environment for this toolbox is explained in Chapter 4. The results of both the simulation and experimental data-sets are also presented in Chapter 4; and the performance of these results is discussed in Chapter 5. All the results presented in this work are implemented in MATLAB. In the end, the findings of this thesis are concluded in Chapter 6. The experimental data-set of a mouse brain is obtained at Erasmus MC, Rotterdam.

1.1 Image Acquisition

The data recorded by the linear transducer array is processed as per the stages described below and is illustrated in Figure 1.2.

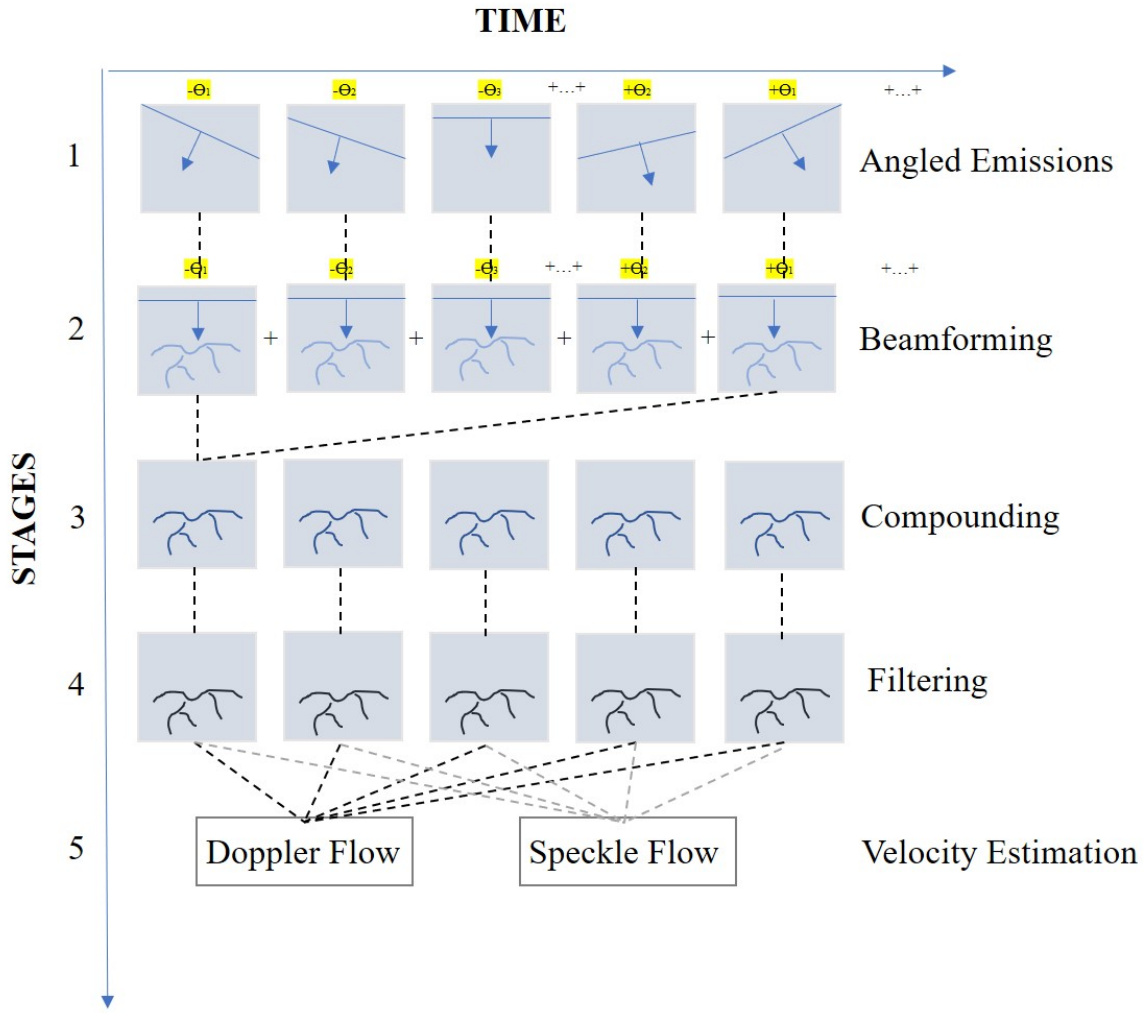

Figure 1.2: Overall flow map depicting the stages from the raw data recording until the velocity estimation. Stage one depicts the repeated firing of plane waves in a sequence of unique angles; Stage two aligns the angle plane waves with the transducer axis and calculates the spatial response by focusing the waves; Stage three shows the compounding i.e the addition of all the beamformed frames in a sequence; Stage four applies high pass filtering on the individual compound frames to eliminate the low frequencies related to the tissue and the respiratory motion; Stage five is where the velocity estimation techniques are implemented.

1.1.1 Angled Emissions

The preliminary step of data acquisition is storing the response of angled plane waves. These plane waves are emitted in an interleaved manner, where emissions are fired at the lowest angle and then increment towards the maximum angle. This whole process is sequentially repeated. A sequence in the raw data acquisition refers to the information received by firing the angled plane waves once for all the unique angles. The backscattered echoes of the m^{th} element coming from the spatial position (z, x) is denoted by $s_m(t_{fm}(z, x), t_s)$. The axis parallel to the linear transducer array is referred as lateral

direction and the axis perpendicular to the array is referred as axial direction.

For the given position (z, x) as shown in Figure 1.3a, the t_{fm} is the time taken by the wave to reach the m^{th} element from the given position. Therefore, it is the sum of the time taken by the plane wave during transmission to reach the given position and the time taken by its reflection to come back from the given position back to the m^{th} element [5]. This time is referred to as *fast-time*. The distance between the position of the element and the given position is denoted by $d_m(z, x)$. The t_{fm} is given by

$$\begin{aligned} t_{fm}(z, x) &= \text{transmitted time} + \text{reflected time}, \\ &= \frac{z\cos\phi + x\sin\phi}{c} + \frac{d_m(z, x)}{c}, \end{aligned}$$

where

$$d_m(z, x) = \sqrt{(z)^2 + (x - x_m)^2}.$$

x_m is the lateral position of the element, c is the speed of sound in the region and ϕ is the inclination angle of emitted plane wave as shown in Figure 1.3b. The elements are placed along the lateral direction where z_m is zero.

t_s is the time stamp at which the plane wave comes back after traversing the complete scanning region. This time is referred to as *slow-time*. The slow time t_s[1] for a plane wave which is emitted at a sequence repetition j with an angle increment n is calculated as

$$t_s(j, n) = (N_{angles}(j - 1) + n)T_{frame},$$

where N_{angles} is the total number of angled plane waves used in a sequence and $n = 1, 2, \cdots N_{angles}$. The total time taken by the planewave to traverse the complete scanning region once is given by T_{frame}. The sampling frequency of the frames is set by $1/T_{frame}$.

[1]For readability, t_s is used instead of $t_s(j, n)$ for equations till beamforming

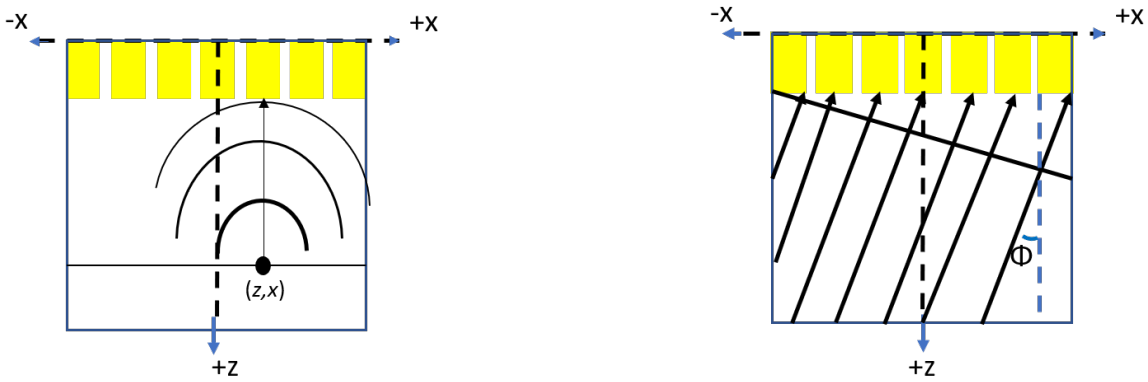

(a) (b)

Figure 1.3: Representation of the spatial coordinates used in the post-processing of the ultrasound acquisition. The rectangular blocks represent the linear transducer array; x-axis indicates the lateral direction; and z-axis indicates the axial direction. In (a) the plane waves reflected from the spatial position (z, x) are shown. In (b) plane waves approach the linear transducer array at an inclination of ϕ.

1.1.2 Beamforming

The beamformed image is produced for each plane wave emission and it provides a complete response of the scatterers at (z, x). The is accomplished by coherently adding the amplitude of the delayed backscattered echoes and is given by

$$BF(z, x, t_s) = \sum_{m=-N/2}^{m=N/2} s_m(t_{fm}(z, x), t_s). \tag{1.1}$$

The spectrum of the real valued beamformed signal in the spatial domain is centered around the ultrasound emission frequency f_0. Hilbert transform is applied on the beamformed signal spatially along the axial direction to demodulate the beamformed signal. Due to the application of this transform, the phase of the positive frequencies is shifted by $-\pi/2$ and the phase of the negative frequencies is shifted by $\pi/2$. The real valued beamformed signal at the is transformed to a complex signal and is given by

$$BF_H(z, x, t_s) = HT_z(\, BF(z, x, t_s)\,),$$

where $BF_H()$ denotes the Hilbert transformed, beamformed signal and $HT_z()$ denotes the Hilbert Transform function applied to the axial direction. The complex values are required to calculate the envelope of the signal and to compute the velocities of the scatterers in the scanning region using the Doppler method. The phase of the complex value helps in determining the sign of the frequency. The phase content is crucial for the Doppler method to work.

1.1.3 Compounding

The values at all spatial positions for a given slow-time stamp is referred to as a frame. The beamformed frames of a sequence are added together to form a compounded frame. Now, it is required to show the independent variables of t_s as $t_s(j,n)$ because a compounded frame is formed by adding the Hilbert transformed, beamformed frames for the total number of angled plane N_{angles} as

$$CF(z,x,t_s(j,N_{angles})) = \sum_{n=1}^{N_{angles}} BF_H(z,x,t_s(j,n)).$$

From now onward, the compounded frame would be denoted as $CF(z,x,t_s(j))$. The N_{angles} is a constant term and therefore could be removed from the compounded frame notation.

1.1.4 Filtering

In the slow-time dimension, it is important to apply a clutter filter [4] at every pixel to reject the low frequencies corresponding to the global motion and the respiratory motion of the scanning region. The filtering operation tends to extract the blood activity response that corresponds to the high frequencies. A Butterworth high pass filter is used for this purpose and the filtered, compounded frame consisting of blood motion is denoted by $CF_b(z,x,t_s(j))$.

1.1.5 Velocity Estimation

After the filtering process, the compounded frames are ready to be used for velocity estimation techniques. The velocity estimation techniques, namely, the Doppler method [6] and speckle tracking [7] are discussed in detail in Chapter 2. These two methods are merged together to develop an improved velocity estimator which is discussed in 3.

1.2 Doppler Imaging

Doppler imaging is based on the well-known concept of physics known as the Doppler effect. The Doppler effect states that a stationary observer will experience a change in the perceived frequency depending on the direction and speed of the transmitting wave source. If the transmitting wave source is moving towards the observer then there is an increase in the received frequency whereas if the transmitting source is moving away from the observer then there is a decrease in the received frequency in relation to the position of the stationary observer. In ultrasound, the transducer is the source where the movement of the scatterers in the scanning region is found by measuring the change in the phase value of the reflected source waves. The change in the phase value is generally interpreted as the change in the percieved frequency which is known as *Doppler frequency*. The activity of scatterers is found using the Doppler frequency and can be visualized by the following sub-modes[2]:

[2]These sub-modes are explained with respect to the brain imaging using ultrafast ultrasound

- Power Doppler Imaging
- Signed Power Doppler Imaging
- Color Doppler Imaging

1.2.1 Power Doppler Imaging

The amount of red blood cells per volume of the scanning region is represented as the brightness map in the Power Doppler Image (PDI) [4]. The PDI is formed when the filtered frames are averaged over a time range. The average value represents the average power of the Doppler frequency. This time range is decided by the consistency of the blood flow dynamics. The number of frames used to compute the brightness map of the PDI is termed as the *ensemble length*. The PDI value at each spatial position is the summation of the squared absolute values over the ensemble length $N_{ensemble}$. The PDI computation is given as

$$PDI(z,x) = \frac{\sum_{j=1}^{N_{ensemble}} |CF_b(z,x,t_s(j))|^2}{N_{ensemble}}.$$

1.2.2 Signed Power Doppler Imaging

This mode of imaging superimposes the directional information of the flow over the PDI. The sign of the present Doppler frequencies indicate the direction of the blood flow. The positive sign means that the flow is towards the placement of the transducer and vice versa for the negative sign [8]. The direction of flow in the vessels can be visualised by taking the sum of the power spectral densities separately for the positive and negative spectrum. The Power Spectral Density (PSD) of $CF_b(z,x,t_s(j))$ in slow-time is denoted by absolute square of its Fourier coefficient $\hat{CF}_b(z,x,\omega_s(j))$. The PSD is given by

$$S(z,x,\omega_s(j)) = |\hat{CF}_b(z,x,\omega_s(j))|^2.$$

The signed Power Doppler images at each spatial position are computed as

$$PDI_+(z,x) = \sum_{j=1}^{N_{ensemble}/2-1} S(z,x,\omega_s(j)), \text{ and}$$

$$PDI_-(z,x) = \sum_{j=N_{ensemble}/2+1}^{N_{ensemble}} S(z,x,\omega_s(j)).$$

1.2.3 Color Doppler Imaging

The Doppler frequency is directly proportional to the velocity of blood particles in a vessel. The positive frequencies indicate that the velocities are directed towards the location of the transducer array and vice versa. The signal at each position (z,x) is transformed in its frequency domain to compute the power spectrum over its ensemble

length. The frequency corresponding to the average of the power spectrum gives the Doppler frequency [8], computed as

$$f_d(z,x) = \frac{\sum_{j=1}^{N_{ensemble}} \omega_s(j) \sum_{j=1}^{N_{ensemble}} S(z,x,\omega_s(j))}{2\pi \sum_{j=1}^{N_{ensemble}} S(z,x,\omega_s(j))}.$$

Color Doppler imaging relies on the computation of flows whereas Power Doppler imaging relies on the average power which makes PDI more sensitive to the different directions of the flow than the Color Doppler image.

1.3 Current Issues with Doppler Imaging

The idea behind Doppler imaging in ultrasound is to map the response of blood flow in the brain vessels. The true velocity measurement is obstructed due to the following issues.

Out of plane motion

The brain consists of vessels running in all three spatial dimensions. When a two-dimensional sector is scanned using the linear transducer, the measured velocity is equal to the projection of the velocity vector in the two-dimensional plane. This obscures the measurement of the true velocity.

Directional sensitivity

The sensitivity of particle movement in the scanned region is highest in the perpendicular direction to the linear array and the sensitivity decreases as the angle between the line perpendicular to the array and the velocity vector increases.

Aliasing

The time taken to record one sequence of angled emissions is termed as Pulse Interval Time (PIT). The reciprocal of the PIT gives the Pulse Repetition Frequency (PRF). High PRF means a high number of frames can be captured in one second, increasing the maximum detectable velocity using the Doppler method. PRF is dependent on the size of the imaging domain and the central frequency of the emitted ultrasound wave. Velocities higher than the Nyquist limit maps in the spectrum of negative frequencies which results in false-negative velocities. The mapping of higher positive velocities onto the negative velocities is called *Aliasing*.

We will now concentrate on the information provided by Power Doppler Imaging and couple its advantages with the speckle tracking to provide accurate estimates of the blood velocity in the brain. This is done to tackle the issues related to the directional sensitivity and aliasing. So far, speckle tracking is vastly used in heart applications as flow occurs in arteries of large diameters making the implementation of the speckle techniques quite effective. When applied to the brain, the convoluted structure of brain

vessels should be considered. The working of the Doppler method and speckle tracking method is discussed in detail in the next chapter.

Directional Velocity Estimation Methods

2

Blood velocity estimation in ultrasound broadly relies on Doppler and the speckle flow measurement techniques. In clinical practice, blood flow measurements inside the brain is limited to one dimensional Doppler imaging [4]. This opened research areas for multi-dimensional blood flow estimators using speckle tracking and Doppler Processing. Different setups of transmission and reception methods of ultrasonic waves like Planewave Transverse Oscillation, Compounded Plane waves, and Multi direction Velocity Estimation [1] allow for a better quantization of the multi-dimensional flow. In this thesis, we will focus on estimating the two-dimensional velocity vector for Ultrafast Ultrasound by combining the merits of Doppler imaging with speckle tracking. This Chapter introduces the working concepts and equations of these two techniques in Sections 2.1 and 2.2 respectively, along with the potential they behold to estimate better velocity vectors.

2.1 Doppler method

In Ultrasound, the Doppler frequency provides the frequency corresponding to the velocity of scatterers. The concept of Doppler imaging is explained in Chapter 1. Here, a generic example is considered to derive the Doppler frequency formula. An ultrasonic wave with the central frequency f_0 is emitted by one transducer element to observe the movement of scatterers within the target area in the scanning region. The ultrasonic wave consists pulses of finite length. The Doppler frequency is calculated by emitting the wave repeatedly at a sampling frequency f_s. The target area under the observation is highlighted by the dashed line in Figure 2.1 which shows the change in the phase between the emitted plane waves due to the movement of the scatterers.

In Figure 2.1, the phase shift in the plane waves emitted at f_s is shown. In one element transducer array, the scatterers movement is seen only in the axial direction. Since there is one element of the transducer, the beamforming operation is not required. The recorded response is a real valued signal which is converted to a complex valued signal by applying the Hilbert transform. The complex recorded signal is given by

$$r(n) = A_n \exp\left(\frac{i2\pi f_d n}{f_s}\right),$$

where n is the count of emissions, f_d is the Doppler frequency and A_n is the magnitude of the recorded response. A discrete Fourier transform is applied on $r(n)$ to compute the f_d. At f_d, the average power of the signal is concentrated. The Doppler velocity v_d is derived from f_d. The scatterers would have moved by a distance z when the second transmitted wave reaches the target area as shown in Figure 2.1. The change in the phase of the backscattered echo due to this movement is given by $\Delta(\phi)$. The

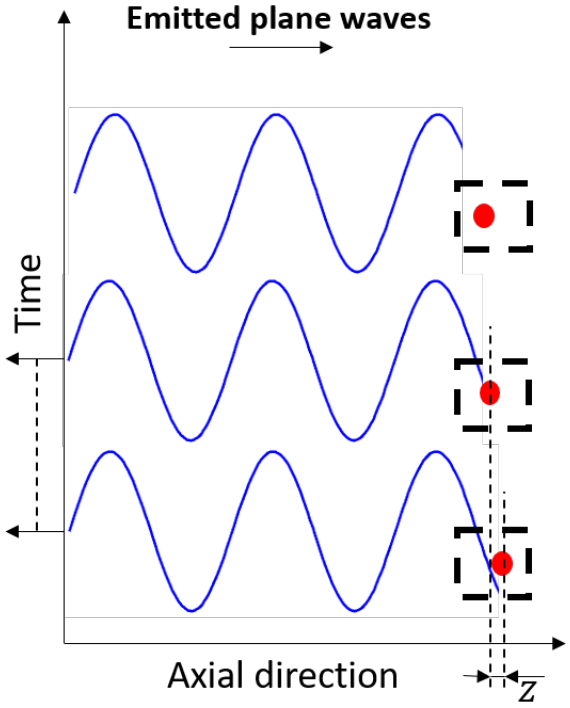

Figure 2.1: Visualization of the Doppler frequency for a one element ultrasound system. The vertical axis indicates the slow-time emission of the plane waves. The horizontal axis indicate the spatial position of the scanning region which is the axial direction in this case. To estimate the movement of scatterers (shown in the solid red circle) z in the target area (boundary marked by the dashed line), the ultrasonic waves are repeatedly emitted at a sampling frequency f_s. The target area is the size of one imaging pixel. It can be seen that the movement of the scatterers causes a phase shift in the emitted plane waves.

ratio of the phase change with respect to the complete phase cycle is equal to the ratio of total moved distance $2z$ with respect to the wavelength λ_0 of the ultrasonic wave. The total distance moved by the scatterers is considered during both the emission and transmission time taken by the plane wave. The equality of the ratios is given by

$$\frac{\Delta(\phi)}{2\pi} = \frac{2z}{\lambda_0},$$

where $z = v_d/f_s$ and $\lambda_0 = c/f_0$. The speed of sound is c in the scanning medium. The above equation can be rewritten as

$$\frac{\Delta(\phi)}{2\pi} = \frac{2v_d f_0}{cf_s}.$$

Hence, the Doppler velocity is

$$v_d = \frac{cf_s\Delta(\phi)}{4\pi f_0},$$

where the Doppler frequency is given by

$$f_d = \frac{f_s \Delta(\phi)}{2\pi}.$$

The Doppler frequency is based on the sampling frequency. In Ultrasound imaging of the brain, the Doppler frequency at each spatial position is computed in slow-time. The compounded frames are produced in the slow-time where the number of compounded frames per second sets the sampling frequency for which the Doppler frequency is calculated. The cardinal method for calculating the Doppler frequency is to take the Fourier Transform of the slow-time ensemble at each spatial position and then compute its average frequency. An effective approach in finding the Doppler frequency is to use the Lag-One Autocorrelation method as explained in [6].

2.1.1 Implementation using Lag-one Autocorrelation method

This method computes the Doppler frequency using the autocorrelation of the time domain values. The equations that convert the autocorrelation estimate to a velocity estimate are explained below.

According to the Wiener Khinchin theorem, the autocorrelation in the time domain is the inverse Fourier Transform of its Power Spectral Density (PSD) estimate. Therefore, the Lag-one Autocorrelation can be written as

$$R(1) = \frac{1}{2\pi} \int_{-\pi}^{\pi} S(z, x, \omega) \exp(i\omega) d\omega,$$

where $S(z, x, \omega)$ is the PSD estimate of the filtered compounded signal $CF_b(z, x, t)$ at the spatial position of (z, x). The PSD estimate is the squared magnitude of $\hat{CF}_b(z, x, \omega)$ (Fourier transform of the $CF_b(z, x, t)$), given by

$$S(z, x, \omega) = |\hat{CF}_b(z, x, \omega)|^2,$$

where

$$\hat{CF}_b(z, x, \omega) = \int_{-\infty}^{\infty} CF_b(z, x, t) \exp(-i\omega t) dt.$$

If the PSD is at an angular frequency ω_d (which corresponds to a phase shift $\Delta(\phi)$), such that $S(z, x, \omega) = \delta(\omega - \omega_d)$, the autocorrelation function is

$$\begin{aligned} R(1) &= \frac{1}{2\pi} \int_{-\pi}^{\pi} \delta(\omega - \omega_d) \exp(i\omega) d\omega, \\ \implies R(1) &= \frac{1}{2\pi} \exp(i\omega_d). \end{aligned}$$

Here, the argument of R(1) is multiplied with the slow-time sampling frequency to give the Doppler frequency in (2.1). When the ultrasonic wave has central frequency f_0, the Doppler frequency at (z, x) is

$$f_d(z,x) = \frac{f_s}{2\pi} arg\{R(1)\}, \tag{2.1}$$

where f_s is the slow-time sampling frequency of $\tilde{CF}(z,x,t)$. The Doppler velocity at the spatial position (z, x) is

$$v_d(z,x) = \frac{c f_d(z,x)}{2 f_0}. \tag{2.2}$$

The Lag-one method is computationally faster and has higher accuracy than the Fourier Transform based method.

In the Doppler velocity estimation, if the particle is moving in a direction perpendicular to the direction of the plane wave this method renders futile results. Figure 2.2 shows the Doppler flow estimation for simulated vertical and horizontal vessels. The actual velocity of the flow of both the vessels is 0.3m/s. The velocity estimation for the vertical vessel is comparable to that of the actual velocity but the same does not hold in the case of the horizontal vessel. The vessel's boundary is highlighted at the centre. From Figure 2.2, the Doppler velocities in the same within and outside the vessel. This happens because only the phase of the Doppler frequency is considered and not its amplitude.

As explained in Chapter 1, a Power Doppler Image (PDI) which is the mean of average Doppler frequencies gives a mean response of blood activity over the ensemble length. This is turn provides the spatial information of the blood vessels present in the scanning region. Though, the Doppler method cannot be used as a velocity estimator due to its ill response in the lateral direction but it can be used to extract the location of the vessels.

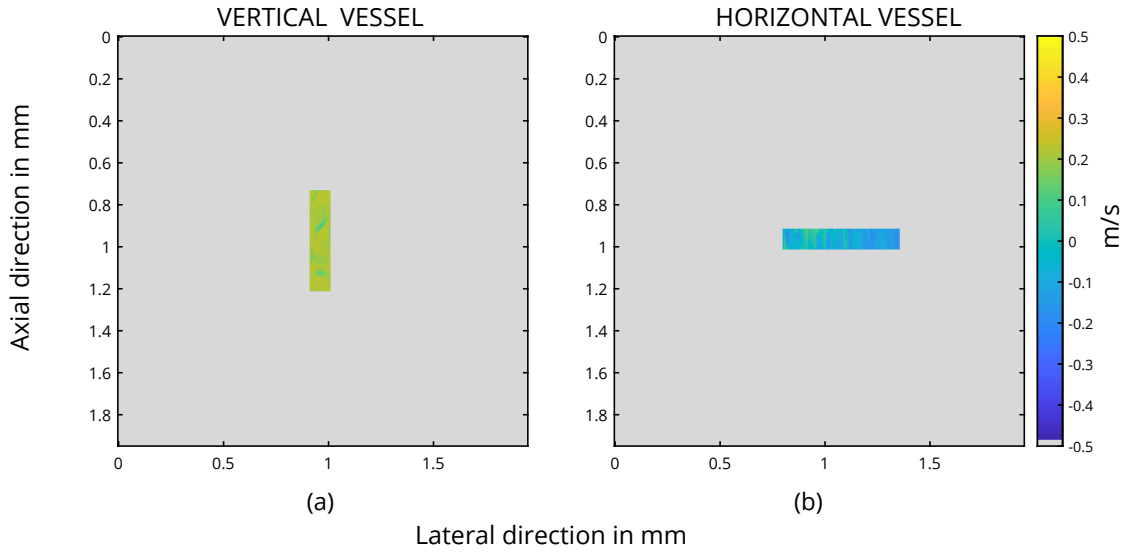

Figure 2.2: Velocity estimation of the scanning region using the Doppler method. The y-axes indicates the axial direction and the x-axes indicates the lateral direction of the region. The axial velocity is indicated by the brightness map. In (a), the area at the centre contains the simulated flow of 0.3m/s in the decreasing axial direction and in (b), the area at the centre contains the simulated flow of 0.3m/s in the increasing lateral direction. The Doppler estimates of the vertical vessel simulation show comparable values to the actual flow whereas the estimates are ineffective for the horizontal vessel simulation.

2.2 Speckle Tracking method

The interference of waves with the granular structure in the scanning medium results in the visualization of speckle. The speckle pattern moves when the particles in the medium move. The speckle pattern remains correlated for consecutive frames but is uncorrelated for a longer duration of time. The method by which the motion of particles can be estimated using the knowledge of speckle displacement is called speckle tracking [9]. In speckle tracking, two consecutive images are compared with each other to find the displacement vectors in the horizontal and vertical directions of the image.

The block matching technique based on the maximization of Normalized Cross-Correlation (NCC) has been used for speckle tracking [1] [10]. In this block matching technique, images are divided into blocks as shown in Figure 2.3 and then each pair of corresponding blocks between two frames is used to find the velocity vector. Therefore, one velocity vector represents the flow information for each block. The number of velocity vectors in a frame depends on the size and overlap between the blocks. The minimum block size should be such that it encompasses the whole structure of a speckle, else the velocity vector will give random values. The maximum velocity that can be detected depends on the size of the block. The implementation of NCC is provided in the following subsection.

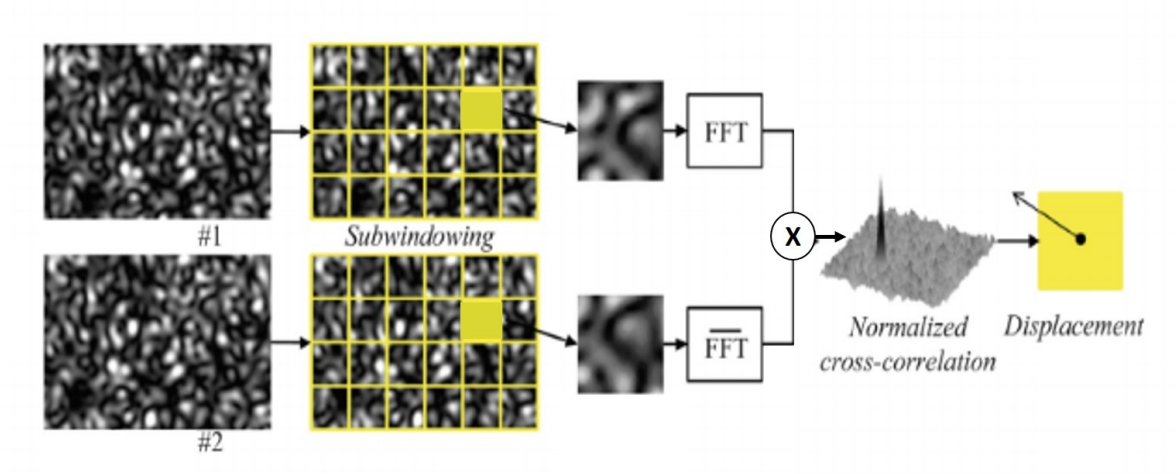

Figure 2.3: Flowchart of a speckle tracking algorithm using NCC. Firstly, two subsequent frames are divided into blocks (also known as subwindowing step); then NCC is calculated for the corresponding block pairs by normalizing the Fourier Transforms of the blocks; finally, the displacement vector is measured by finding the peak corresponding to the maximum of the correlation map. This is a modified figure from [9].

2.2.1 Implementation using Normalized Cross-Correlation

A general algorithm for NCC as outlined in [1] is divided into three steps: 1) divide the beamformed images into small blocks; 2) match the block pairs using a similarity or a dis-similarity measure; 3) find the maximum or the minimum displacement of the measure using a peak estimation method. The matching measure used here is used in [9], which calculates the NCC coefficient ρ for the block pairs and finds its maximum to obtain the displacement in these two-dimensional blocks. To find the displaced horizontal and vertical vectors, two successive images p and q are divided, let us say, in a total number of L blocks and the ρ is computed for each block pair (p^k, q^k), where $k = 1, \ldots, L$ is the block number. Using the Fourier Transforms $\hat{p}^k$ and $\hat{q}^k$, ρ for block k is calculated as

$$\rho^k = \frac{\mathcal{F}^{-1}(\overline{\hat{p}^k}\hat{q}^k)}{MN\sigma_p^k\sigma_q^k}.$$

$\overline{\hat{p}^k}$ represents the complex conjugate of the Fourier Transform of $\hat{p}^k$, MN represents the size of the block in pixels and σ is the standard deviation of this stochastic process.

The subpixel displacements in vertical z and horizontal x directions are found by estimating the peak of ρ^k using parabolic curve-fitting. The displacement is found as

$$(\Delta z_{p\to q}^k, \Delta x_{p\to q}^k) = \max(\rho^k). \tag{2.3}$$

When speckle tracking using NCC is implemented to detect the blood flow in the brain vessels, the performance is found to be poor. As shown in Figure 2.4, where the

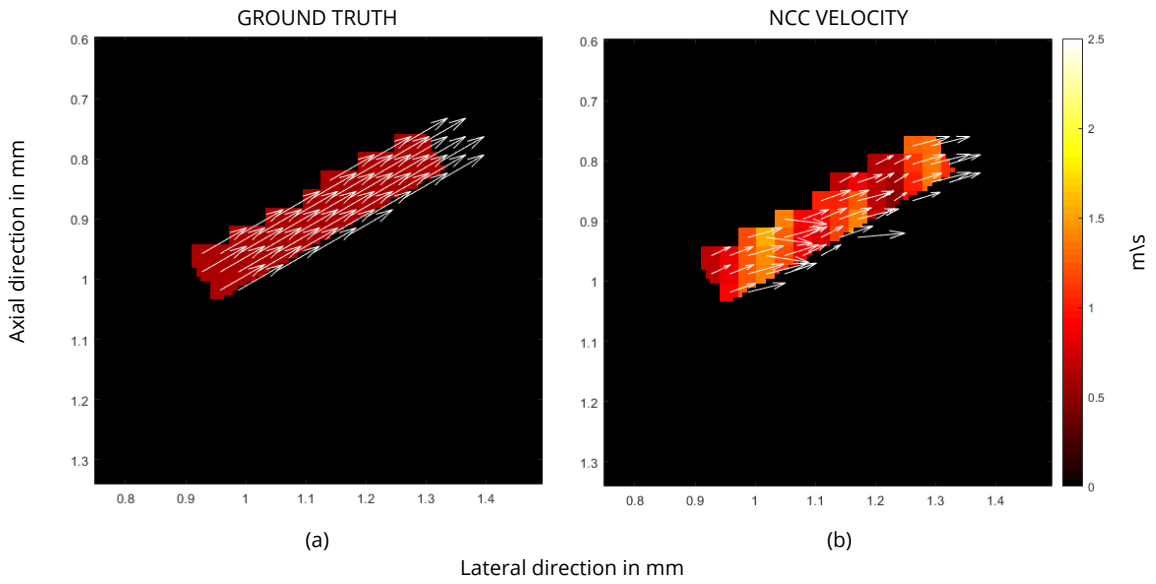

Figure 2.4: The simulated vessel is inclined at 30° consisting of ground flow velocity of 0.6m/s. The velocity magnitude at is displayed at each pixel by the colorbar on the right side. The arrows over the magnitude plot display the direction of the flow and the length of the arrow is directly proportional to the magnitude. (a) shows the actual velocity and (b) shows the velocity computed using the standard NCC (implemented in MATLAB). It is seen that some of the NCC vectors show false velocity directions. The ultrasound data-set for this simulation is obtained using the k-Wave toolbox [11] (further details of the setup are given in Chapter 4).

speckle tracking is implemented on the simulated k-Wave data-set, this method works poorly for the narrow vessels. In this figure, the left image shows the ground velocity magnitude using a colormap and the direction of actual velocity using arrows over the region of the vessel. Similarly the right image shows the magnitude and direction of the velocity vectors which were computed by implementing the NCC algorithm in MATLAB.

As opposed to the Doppler method, speckle tracking can find the vector flow in all directions as demonstrated in [12].The performance of speckle tracking in the brain can be improved if the speckle matching process can be guided along the vessel's curvature. This is done by using prior information in the form of the vessel's orientation to guide the speckle matching process as discussed in Chapter 3.

3 Proposed Methodology

Two categories of velocity estimation techniques were discussed in the last chapter. Moving forward in this Chapter, a new method is proposed where the merits from both the techniques are combined to estimate the blood flow in the brain. Here, the orientation of the vessel which is obtained through the segmentation of the Power Doppler Image acts as prior information to increase the accuracy of the velocity estimation. The constraint enforces the velocity estimator to find the vector along the direction of the vessel. As explained in Chapter 2 velocities between two frames are estimated when a block in one frame is matched to the corresponding block in the second frame. The directional constraint in the matching procedure of speckle tracking is used along with the framework of the Orthogonal Matching Pursuit (OMP) [13]. The implementation of OMP with the directional constraint is called GOMP. The steps developed for calculating the orientation of the brain vessels are discussed in Section 3.1. A system model for speckle tracking is formulated in Section 3.2 and the implementation of GOMP on the system model is explained in Section 3.3. The computation of the directional constraint in the form of spatial weights is in Section 3.4. The overall procedure adopted to estimate the blood velocities using GOMP is given in Section 3.5.

Notation: A vector, say $\mathbf{x}$ is represented by a small alphabet in bold font. An element in the i^{th} position of a vector is symbolized by x_i. Matrix notation is given by a bold capital font like $\mathbf{X}$, while a column of matrix $\mathbf{X}$ is given by $\mathbf{x}_i$.

3.1 Orientation of the Vascular Map

The Power Doppler Imaging helps in visualizing a vascular network of the brain. The orientation of the vessels can be extracted from the PDI to be used as prior information in the calculation of finding the velocity vectors within the vessel's curvature. As shown in Figure 3.1, in contrast to the standard speckle tracking techniques where the probability of finding the vectors is equal in all the directions, the proposed speckle tracking has higher probabilities along the vessel's orientation. A method to extract the orientation of the vessels is developed so the probabilities based on vessel's curvature can be calculated. The probabilities are used in the form of spatial weights which are explained in Section 3.4.

Figure 3.2 shows the process of extracting the orientation of the vessels from the PDI of the cerebellum region of the mouse brain. The detailed information behind the acquisition parameters of the mouse data is discussed in Chapter 4. Firstly, the PDI is segmented to separate the vascular network from the background. The segmentation is done by finding a uniform threshold value through a trial and error approach in which the values higher than the threshold value in the PDI are kept and the others are discarded. A two-dimensional first-order differentiator is applied to the segmented

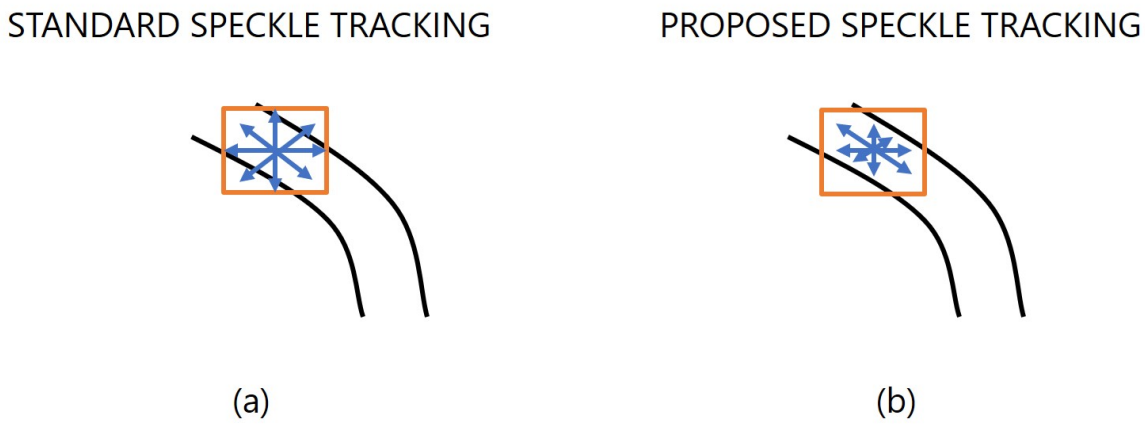

Figure 3.1: (a, b) displaying the difference in the approach of the standard and the proposed speckle tracking methods, respectively. The blue arrows indicate the possible flow directions within the vessel and the length of the arrow shows the probability of finding that direction. In (a), the probability of finding the velocity estimates is maintained same in all the directions for a standard speckle tracking technique. In (b), the directional probability is non-uniform and is maximum within the curvature of the vessel.

PDI to find the raw orientation of the vessels. The first-order differentiator does not work within the vessel's area as the PDI intensities within the vessel are almost uniform providing with almost zero gradient changes. As seen from Figure 3.2, the gradients for the raw vessel orientation are significant near the vessel's boundary but almost flat within the vessel's area. In other words, angles measured at the boundaries of the vessels provide a correct measure whereas gibberish angle measures are found within the vessel's perimeter. Therefore, the correct angles at the boundaries of the vessels are extracted using the Sobel edge detector of MATLAB. To get the correct orientation at all the points of the vessels, orientation of the closest extracted boundary is used for each spatial positions.

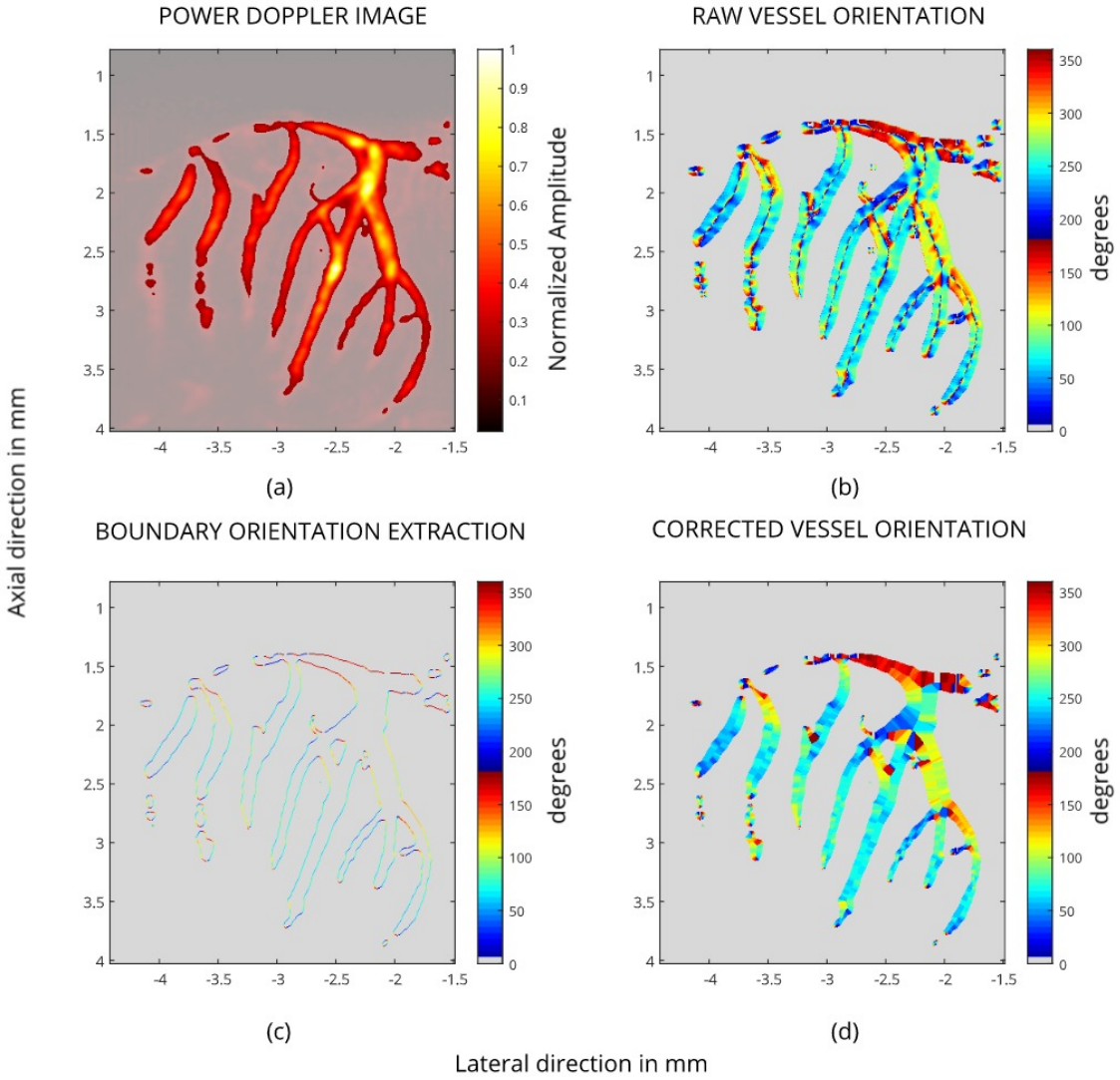

Figure 3.2: Illustration of the steps involved in the computation of the vessel's orientation at each pixel. (a) is the Power Doppler Image (PDI) which is segmented to obtain the location of the vessels. The segmented vessels are passed through the first-order differentiator acting in both the axial and lateral directions. The arctangent of the slope is computed from these differential components to produce the inclination of the pixel in the vessel shown in (b). The vessel's boundaries compute the accurate inclination due to the high contrast between the absence and presence of Red Blood Cells. The boundary values are extracted using the Sobel operator as shown in (c). Finally, the correct orientation values are filled within the vessels at each pixel by finding the orientation of the nearest boundary as shown in (d).

3.2 System Model

The motion of the particles is calculated by finding the displacement of the underlying speckles. Each frame is divided into blocks and each block in a frame is associated with one displacement value. So a block in the frame 1 is matched to all the possible shifted

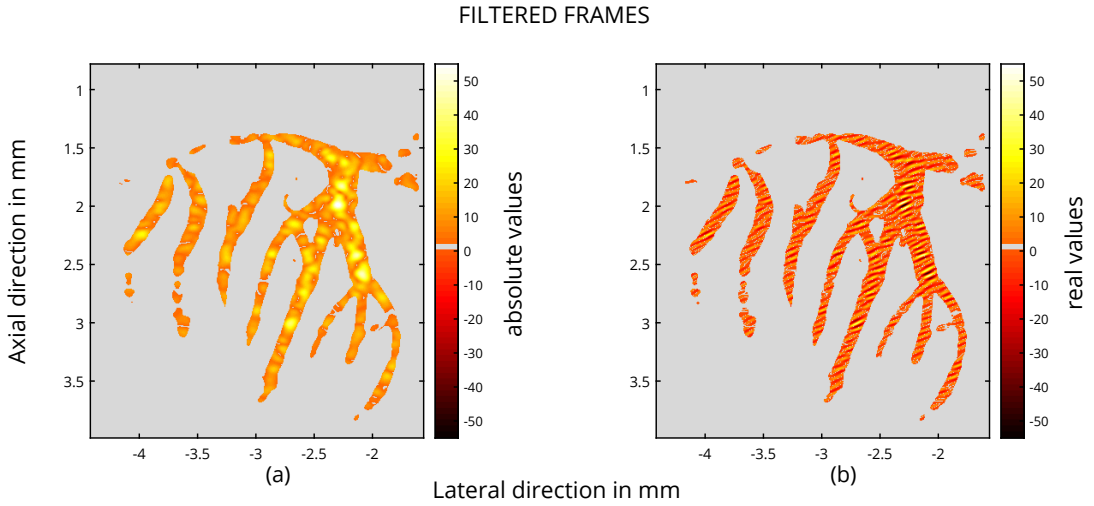

Figure 3.3: Speckle tracking using the proposed method is performed on the real values. (a) shows the absolute signature of a filtered frame and (b) shows the real signature of a filtered frame. The real value is used as it provides discontinuous ridges like pattern which is preferred for the speckle tracking method.

blocks within the search region of the frame 2. The shifted block refers to the block whose centre is present at a shift calculated from the centre of the search region. The shift is measured as a displacement vector between the centre of the shifted block and the centre of the search region. The best match between the two frames is calculated using GOMP. A system model is formulated on which GOMP can be implemented. The speckles of the real valued filtered, compounded frames are tracked. The real values provide a less smooth speckle pattern than the absolute values as shown in Figure 3.3, which is desired for speckle tracking. Therefore, the system model consists only real values.

In Figure 3.4, a block shown in the frame 1 is vectorized as $\mathbf{y} \in \mathbb{R}^M$, where M is the total number of pixels in a block. The shifted blocks in the corresponding search region as shown in the frame 2 are vectorized as $\mathbf{d}_n$, where $n = 1, \cdots, N$. N is the total number of shifts possible in the search region. All the shifted vectors $\mathbf{d}_n$ are stacked column-wise in the matrix $\mathbf{D} \in \mathbb{R}^{M \times N}$, known as the dictionary matrix. The columns of $\mathbf{D}$ are referred to as atoms. The aim of making a dictionary is to construct a matrix that includes all the displaced values of the second frame. The area of the search region in the next frame is decided by the maximum velocity assumed in that region. The objective is to select one column of $\mathbf{D}$ that best matches with $\mathbf{y}$. The selection takes place by forming a selection vector $\mathbf{b} \in \mathbb{R}^N$ to decide which column is of interest. The system equation is given by

$$\mathbf{y} = \mathbf{D}\mathbf{b}. \tag{3.1}$$

As every practical system contains noise, we assume that noise is present in the ultrasound measurement system and is uncorrelated with the measurements. The new system equation is

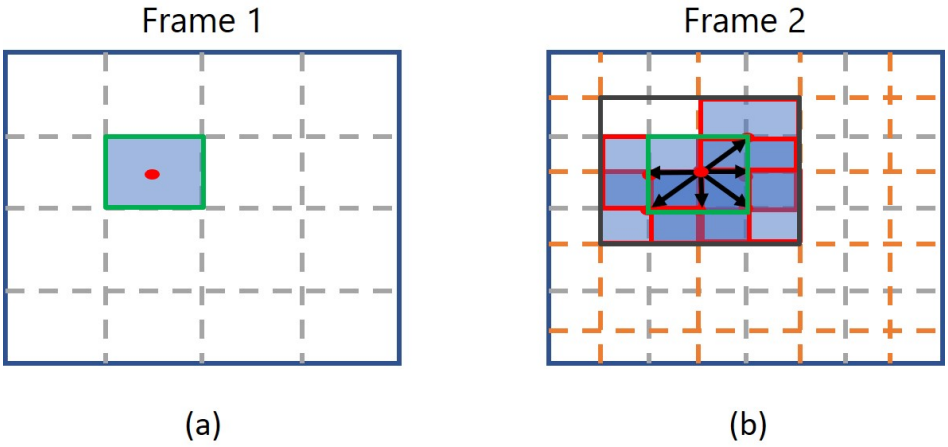

Figure 3.4: The two frames represent the formulation of the system model given in (3.2). In (a), the frame 1 is divided into small blocks indicated by the grey dashed lines. The selected block in the frame 1 is vectorized as $\mathbf{y}$ and this block is searched in the corresponding local search region in the frame 2 (enclosed in the solid black boundaries) in (b). The blocks corresponding to all the shifts (some shifts are shown through the black arrows) are vectorized and stacked column-wise to form a dictionary matrix $\mathbf{D}$.

$$\mathbf{y} = \mathbf{D}\mathbf{b} + \mathbf{n}.$$

One column of $\mathbf{D}$ needs to be found such that it has the highest similarity with $\mathbf{y}$. For the proposed speckle tracking in this thesis, the cardinality k is set to 1. In general for cardinality k the column selection will proceed as

$$\begin{aligned} P_0 : \quad & \min_{\mathbf{b}} \quad \| \mathbf{b} \|_{l_0}, \\ & \text{subject to} \quad \mathbf{D}\mathbf{b} = \mathbf{y}, \ \| \mathbf{b} \|_{l_0} \leq \mathrm{k}, \end{aligned}$$

where $\mathbf{y}$ is the vectorized form of a block in the frame 1 and $\mathbf{D}$ is the dictionary matrix of shifted blocks in the frame 2. The problem P_0 is referred to as a L_0 minimization problem. The computational complexity for P_0 is categorized as a Non-Polynomial Hard (NP-Hard) problem.

To reduce the computational complexity, P_0 can be solved using relaxation methods [14] or greedy methods [13] [15]. The detailed explanation of various approaches to sparse problem modeling along with the theorems that ensure the optimality of these approaches is given in the thesis report of Sejeso [16]. With relaxation methods, the non-convex objective function of P_0 is changed to a convex function and a suboptimal solution for this problem is found. On the other hand, greedy methods search the suboptimal solution by sequentially selecting and storing the basis for the support set of $\mathbf{b}$. This selection criterion reduces the computational complexity to a maximum of cubic order dependencies for the greedy methods. An optimal solution is obtained when matrix $\mathbf{D}$ follows certain conditions [17]. The L_1 relaxation method and greedy methods require the entries of $\mathbf{D}$ to be in accordance with the restricted isometric

condition [18]. The greedy method, namely, Orthogonal Matching Pursuit is used in this thesis to find a column of $\mathbf{D}$ that will provide the best match with the reference $\mathbf{y}$.

The standard Orthogonal Matching Pursuit is modified to compute the displacement between the frames taking into account the orientation of the vessel. The working of this algorithm is explained in the next section.

3.3 Guided Orthogonal Matching Pursuit

The greedy selection of the columns of $\mathbf{D}$ through OMP is described in Algorithm 1. The first step in this method is to find a column of $\mathbf{D}$ which gives a maximum correlation with the residue vector. The residue vector is given by

$$\mathbf{r}(j) = \mathbf{y} - \mathbf{D}\mathbf{b}(j),$$

where j is the iteration number. The columns of $\mathbf{D}$ are indexed by i and are normalized. The i^{th} column is selected by finding the maximum inner product by

$$\max_i |\mathbf{d}_i^\intercal \mathbf{r}(j-1)| \quad \forall i = 1, \cdots, N. \tag{3.2}$$

The i^{th} column that has a maximum correlation, say i_0, with the current residue is added to the support set $\mathrm{S}_j = \mathrm{S}_{j-1} \cup i_0$. Then the least square solution of $\mathbf{b}$ is computed in its current support set S_j and the residue value $\mathbf{r}$ is updated for the next iteration. The iterations are terminated when the residue reach their minimum value

```
1 Initialization ;
2 Iteration Number  j = 0  b(0) = 0  r_0 = y  S_0 = {} ;
3 while r(j) ≤ ε1 or j = k do
4 |   j = j + 1 ;
5 |   Compute i_0 = argmax_i |d_i^T r(j-1)|  ∀i = 1, ··· , N ;
6 |   Update S_j = S_{j-1} ∪ {i_0} ;
7 |   Least Squares b(j) = argmin_b || Db − y ||_2^2  s.t. sup{b} = S_j;
8 |   Update r(j) = y − Db(j) ;
9 end
```

Algorithm 1: Orthogonal Matching Pursuit

or the iterations reach its maximum. The number of iterations is representative of the cardinality of the system k. There are two operations in this algorithm. The first , the least squares operation which finds $\mathbf{b}(j)$ such that the error is perpendicular to the column subspace spanned by the support set S_j; second is the correlation operation where matching is performed between a column of $\mathbf{D}$ and the residue. From these two steps, the method is named as Orthogonal Matching Pursuit. The result is interpreted in the form of selected columns of $\mathbf{D}$. When $k = 1$, the selected index corresponds to the shift of the block in the frame 2. The orientation of the vessel which is computed from the Power Doppler Image could be used to direct the searching of the support set

in the preferred direction, i.e., the direction along the orientation of the vessel. Every column of $\mathbf{D}$ is multiplied by a weight value w_i to guide the searching process. This type of weighing makes the selection of i^{th} column biased towards the orientation of the vessel. The weights depend on the direction of the shift θ_i which is measured by taking the centre of the search region as the origin. The maximization step of the guided matching pursuit is modified to

$$\max_i |w_i.\mathbf{d}_i^\intercal \mathbf{r}(j-1)| \quad \forall i = 1, \cdots, N. \tag{3.3}$$

The weighing of the maximisation step of OMP is referred to as the Guided Orthogonal Matching Pursuit.

3.4 Spatial Weights for GOMP

In [19], three types of weighing functions are defined, namely Cauchy (w_c), Huber (w_h) and Bisquare (w_b) functions. The weight functions are adapted to the GOMP and are given as

$$\begin{aligned} w_c(\theta_i s) &= \frac{2}{1+(\theta_i s)^2}, \\ w_h(\theta_i s) &= \min(1, \frac{p}{|\theta_i s|}), \\ w_b(\theta_i s) &= \left\{ (1 - \frac{(\theta_i s)^2}{c^2})_+ \right\}^2, \end{aligned}$$

where $(a)_+ = \max(0, a)$, s is the scaling parameter and c, p are the hyperparameters. The θ_i ranges from $[-90°, 90°]$. The hyperparameters change the gradient of the weight functions. The scaling parameter tunes the function value according to its domain. The three different weight functions are shown in Figure 3.5, wherein the Bisquare curve smoothly decreases over the domain whereas Cauchy and Huber curves roll down quickly to a minimal weight.

The function value is shifted by the orientation of the vessel θ_v (calculated within the range of $[-90°, 90°]$) as the maximum function value should occur at θ_v. This shift is incorporated in the Huber's weight distribution as

$$w_h((\theta_i - \theta_v)s) = \min(1, \frac{p}{|(\theta_i - \theta_v)s|}), \quad \textbf{if } -90° \leq \theta_i - \theta_v \leq 90°.$$

For GOMP, the Huber distribution is used to compute the spatial weights. Therefore, the weight value in (3.3) is given by

$$w_i = w_h((\theta_i - \theta_v)s).$$

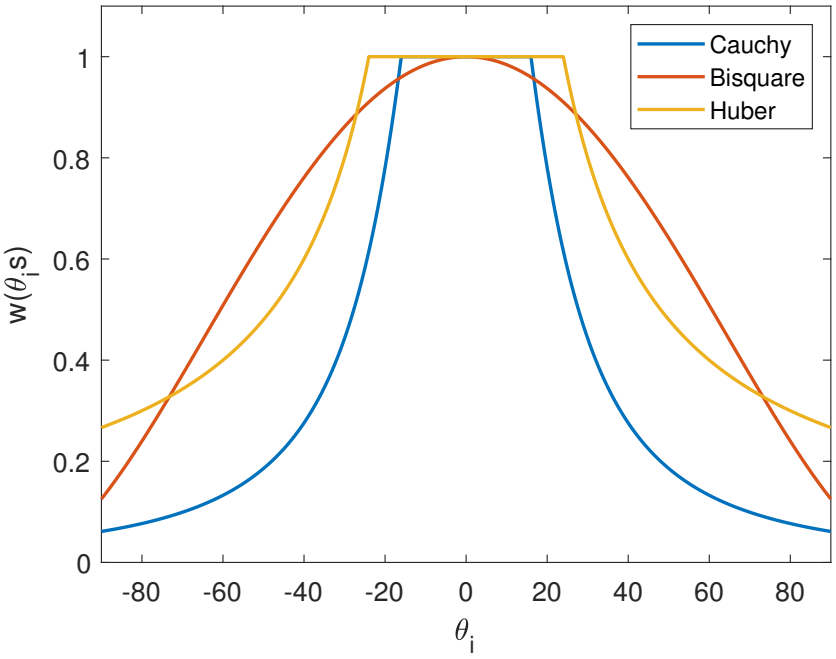

Figure 3.5: Cauchy, Huber (p = 1.5) and Bisquare (c = 7) weight functions are plotted with respect to the angular position θ_i ($s = 1/16$). With these parameters, the Bisquare curve has the smoothest gradient and the Cauchy curve has the maximum gradient over the domain.

Implementation of the spatial weights

The θ_v is the average of the orientation values at each pixel in the selected block of the frame 1. The range of the vessel's orientation lies between -90° to +90°. The implementation of the spatial weights is explained through an example of a vessel that is laterally aligned in the scanning region.

Uniform weights are applied to take into account the possibility of the upward and downward motion of the blood flow in the vessel as shown in Figure 3.6. Therefore, the weights are symmetric around θ_v and $180° + \theta_v$.

A block inside a horizontal vessel is selected as shown in Figure 3.7 and the weights are computed for the different shift directions of this block in the frame 1. The spatial weights at each pixel are obtained from the Huber's function, where the distribution has higher weights for θ_i closer to θ_v and $180° + \theta_v$. θ_v is equal to 0° as the vessel is laterally aligned.

In the next chapter, results are provided on simulated and real data-set which will enable us to verify the accuracy of the proposed method.

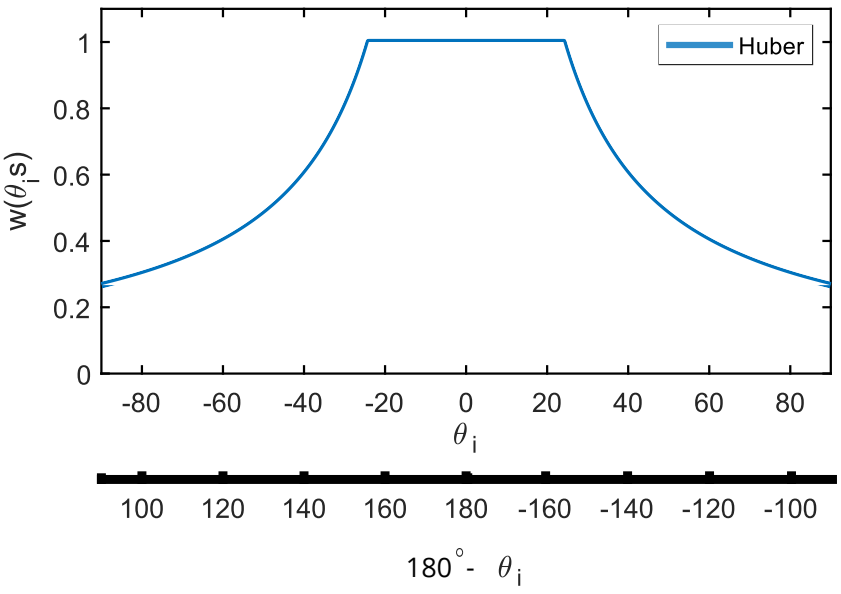

Figure 3.6: Huber function is applied to the horizontal vessel simulation in both the forward and reverse directions. The curve shows the weight distribution for all the angular shifts in the selected block. As θ_v is zero, the spatial weights are uniform for both the forward and reverse flows.

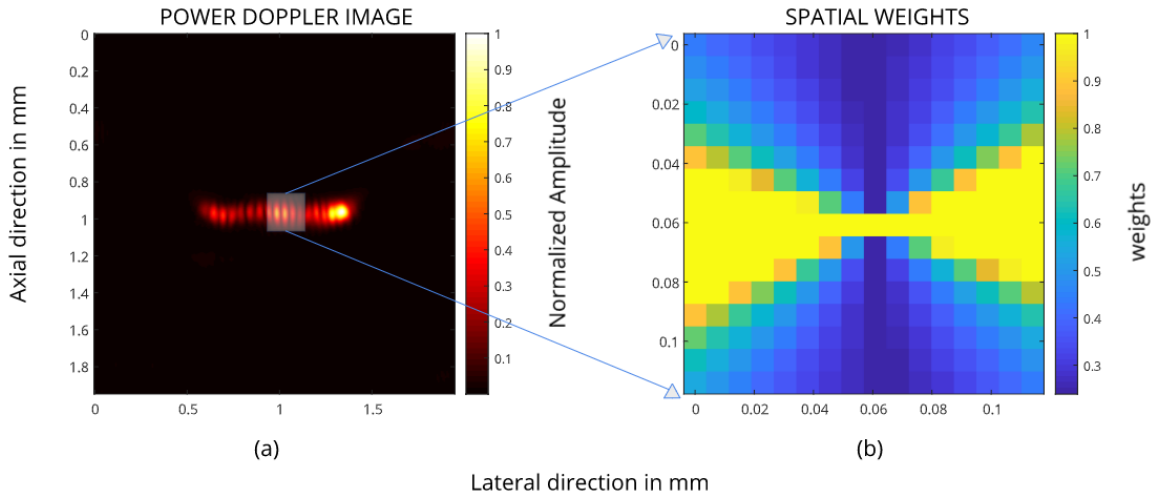

Figure 3.7: The spatial weights distribution for the block placed over the PDI. (a) shows the PDI of a horizontal vessel in the spatial domain. The spatial weights are computed for the block highlighted by the orange boundary. As the vessel's orientation θ_v is zero, the weights for each spatial location in the selected block is shown in (b). Huber function is used to compute these weights.

3.5 Velocity Estimation using GOMP

In this thesis, the velocity vectors for each block are computed using GOMP in the following way:

- The filtered, compounded frames are acquired for an ensemble length $N_{ensemble}$. The total number of frame pairs of the consecutive frames is $N_{ensemble} - 1$. From the estimation theory of signals, the Signal to Noise Ratio of the velocity estimation can be improved if more number of frame pairs are considered. If the number of frame pairs that are considered is n_{avg} then the system model (3.2) is modified to

$$\frac{1}{n_{avg}} \begin{bmatrix} \mathbf{y}_{1,2} \\ \mathbf{y}_{2,3} \\ \vdots \\ \mathbf{y}_{p,q} \end{bmatrix} = \frac{1}{n_{avg}} \begin{bmatrix} \mathbf{D}_{1,2} \\ \mathbf{D}_{2,3} \\ \vdots \\ \mathbf{D}_{p,q} \end{bmatrix} \mathbf{b} + \frac{1}{n_{avg}} \begin{bmatrix} \mathbf{n}_{1,2} \\ \mathbf{n}_{2,3} \\ \vdots \\ \mathbf{n}_{p,q} \end{bmatrix}, \tag{3.4}$$

  where $p = n_{avg}$, $q = n_{avg} + 1$. The subscripts (p, q) of the vectors and the matrices denote the frame pair made up of p^{th} frame as the frame 1 and q^{th} frame as the frame 2.

- The velocity vector is found for k is equal to one. The above system model is used to find a selected index using GOMP. The selected index gives the shift of speckles within a block in the frame 1. According to the sampling frequency of the filtered frames, the velocity vector is calculated from the shift.

- The vectors are estimated for n_{avg} consecutive frame pairs at the each spatial position in the scanning region.

4 Results

The data acquisition parameters for the k-Wave simulation toolbox and the results of the proposed method are presented in this chapter. Section 4.1 consists the settings of the toolbox modules that are used to produce the ultrasonic backscattered echoes from the known components of the scanning region. The Guided Orthogonal Matching Pursuit (GOMP) technique is implemented to find the displacement vectors between the two filtered, compounded frames of the ultrasound acquisition. The spatial weights are combined with the matching pursuit to find the displacement along the direction of the vessel. The weights guide the matching procedure to find the velocity vector within the vessel's curvature as explained in Chapter 3. The sign conventions for velocity estimates is the same as that for the Doppler flow estimates. This means that the direction of the velocities towards the transducer have a positive sign and vice-versa. The sign convention used for the velocities is not the same as that for the spatial positions of the scanning region. Section 4.2 includes the results of velocity estimation using the proposed method and the standard method using Normalized Cross-Correlation (NCC) where the simulation data-set is produced using the k-Wave toolbox. In Section 4.3 the performance of the proposed method is checked on the experimental data-set provided by Erasmus Medical Centre, Rotterdam where the experiments were conducted on a mouse brain.

4.1 Input Structures

In this thesis, the k-Wave toolbox by Bradley Treeby and Ben Cox [11] is used to simulate the behavior of the ultrasound system. This creates a simulation environment that mimics the interaction of plane waves with the moving Red Blood Cells. The details of the toolbox parameters are given in Table 4.1 and the type of the input structures to the k-Wave toolbox is discussed below:

- Transducer: A linear transducer array is defined where each element of the array is excited by a Gaussian pulse. The central frequency of the plane wave emission depends on this Gaussian pulse frequency. An angled plane wave is emitted by sequentially delaying the input pulses to the transducer elements to form a wave front inclined at the given angle with respect to the array axis.

- Computational grid: A spatial grid is defined to calculate the amplitude response of the plane wave interaction with the medium. The horizontal and vertical directions in the imaging region are referred to as lateral and axial directions, respectively. The lateral direction is parallel to the transducer array and the other direction is perpendicular to the transducer array.

TABLE 4.1. THE PARAMETERS OF THE ULTRASOUND SETUP IN THE K-WAVE SIMULATION

Transducer		**Grid**		**Medium**	
Excitation	Gaussian	**Lateral length**	256 pixels	**Tissue density**	1041 kg/m^3
Central Frequency	25 MHz	**Axial length**	256 pixels	**Tissue sound speed**	1541 m/s
Pitch	7.6 μm	**Resolution**	7.6 μm	**Blood density**	$\sim \mathcal{N}(1041, 40)$ kg/m^3
Kerf	0 μm	**Grid size**	1.9 mm x 1.9 mm	**Blood sound speed**	$\sim \mathcal{N}(1541, 40)$ m/s

- Medium: The medium properties are defined by the density and speed of the sound of the medium to be scanned. The background region resembles the tissue region and the vessel region resembles the Red Blood Cells.

4.2 Simulation Results

Three different versions of simulations are produced to compare the accuracy of the proposed method with NCC. The first version contains blood flow inside a vertical vessel that is perpendicular to the transducer array; the second version contains flow inside a horizontal vessel that is parallel to the array and the third version contains flow inside a slanted vessel that makes an angle of 30° with the array axis. The true velocity of particles inside the vessels is kept constant throughout the simulation time. A sequence of five angled plane waves $[-10^\circ\ -5^\circ\ 0^\circ\ 5^\circ\ 10^\circ]$ is repeated to obtain 60 compounded frames ($N_{ensemble} = 60$). With the simulation parameters in Table 4.1, the sampling frequency at which a plane wave is emitted would be 363kHz in a real-time scenario. In these simulations the sampling frequency of compounded frames is high because the emitted plane waves scan a small region with dimensions of 1.9mm $\times$ 1.9mm, hence covering the scanned area at a faster rate. A high pass Butterworth filtering operation is applied to the compounded frames where the cut-off frequency is set as two percent of the sampling frequency and the order of the filter is set as 8. The filtering operation ensures that the amplitude of the stationary and slow moving tissue is removed from the ultrasound signal to track the amplitude of the moving Red Blood Cells. A block size of 16 $\times$ 16 pixels is chosen as it is large enough to enclose the complete outline of speckles. The velocities in the axial and lateral directions for each version is given in Table 4.2. The positive axial velocities point towards the transducer and the positive lateral velocities point towards the increasing spatial position in the lateral direction. The number of compounded frame pairs n_{avg} considered to calculate the displacement vectors is 4.

The results for the simulation are given in the below-mentioned order. Foremost the Doppler velocity estimation at each pixel of the scanning region is shown for each version; then the computation of the spatial weights for these versions is shown; followed by the frame-wise velocity estimation which shows the velocity components per n_{avg} frame pairs; and then the final velocity estimation for the complete ensemble length of the 60 filtered frames. Lastly, the convergence analysis compares the quality of the velocity magnitudes in the axial and lateral directions computed by the NCC and the proposed method.

TABLE 4.2. AXIAL AND LATERAL VELOCITIES SET AS REFERENCE IN THE K-WAVE SIMULATION FOR THE THREE VERSIONS

Ground Truth	Vertical Vessel	Horizontal Vessel	Slanted Vessel
Axial Velocity (m/s)	0.3	0	0.3
Lateral Velocity (m/s)	0	0.3	0.52

4.2.1 Doppler Velocity

The performance of the Doppler blood flow estimation is analyzed in this subsection. The Doppler velocity is calculated using the Lag-One Autocorrelation [20] for the ensemble length of 60 filtered frames. Figure 4.1 shows the estimates for all the three versions. The Doppler estimation in the vertical vessel is close to the ground truth but this method does not appropriately work for the slanted vessel and the horizontal vessel. In the slanted version, the overall axial velocity is closer to the actual vertical component. The axial velocity is close to zero in the horizontal vessel version. As the Doppler estimation is suitable in the planewave emission direction, it provides comparable velocity estimates only for the vertical vessel simulation; lower overall velocity estimates for the slanted vessel simulation and approximately zero estimates for the horizontal vessel simulation.

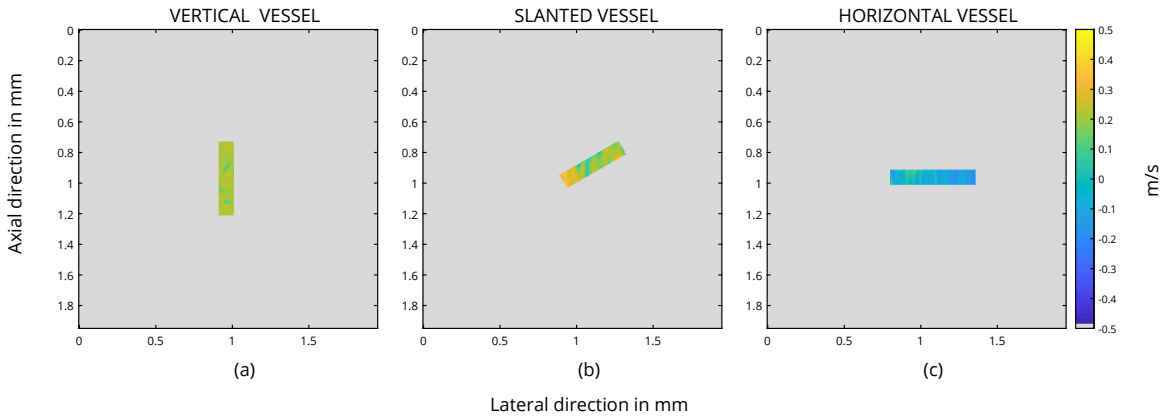

Figure 4.1: The axial velocities for the three simulated versions computed using the Lag-One Autocorrelation. The centre of the images show the area of the vessel. (a) is the Doppler flow estimation of the vertical vessel, (b) is of the slanted vessel and (c) is of the horizontal vessel. The ensemble length for the Doppler estimation is 60. The actual flow velocities are given in Table 4.2. The Doppler estimation is accurate for the vertical vessel simulation, lower than the actual magnitude for the slanted vessel simulation and inaccurate for the horizontal vessel simulation.

4.2.2 Spatial Weights

The velocity vectors are obtained in the narrow vessels with the usage of the spatial weights. The spatial weights are computed from the segmentation of the Power Doppler Image (PDI). The PDI is obtained after averaging the 60 filtered frames and provides

the location of the vascular network in the scanned region. After applying image segmentation, the vessel masks are obtained from the PDI. With the angle detection technique discussed in Chapter 3, the orientation of the vessels is found. In Figure 4.2, the first column shows the PDI of each vessel; the second column shows the orientation of the vessels; and the third column shows the distribution of the spatial weights defined for the selected block in the filtered frame.

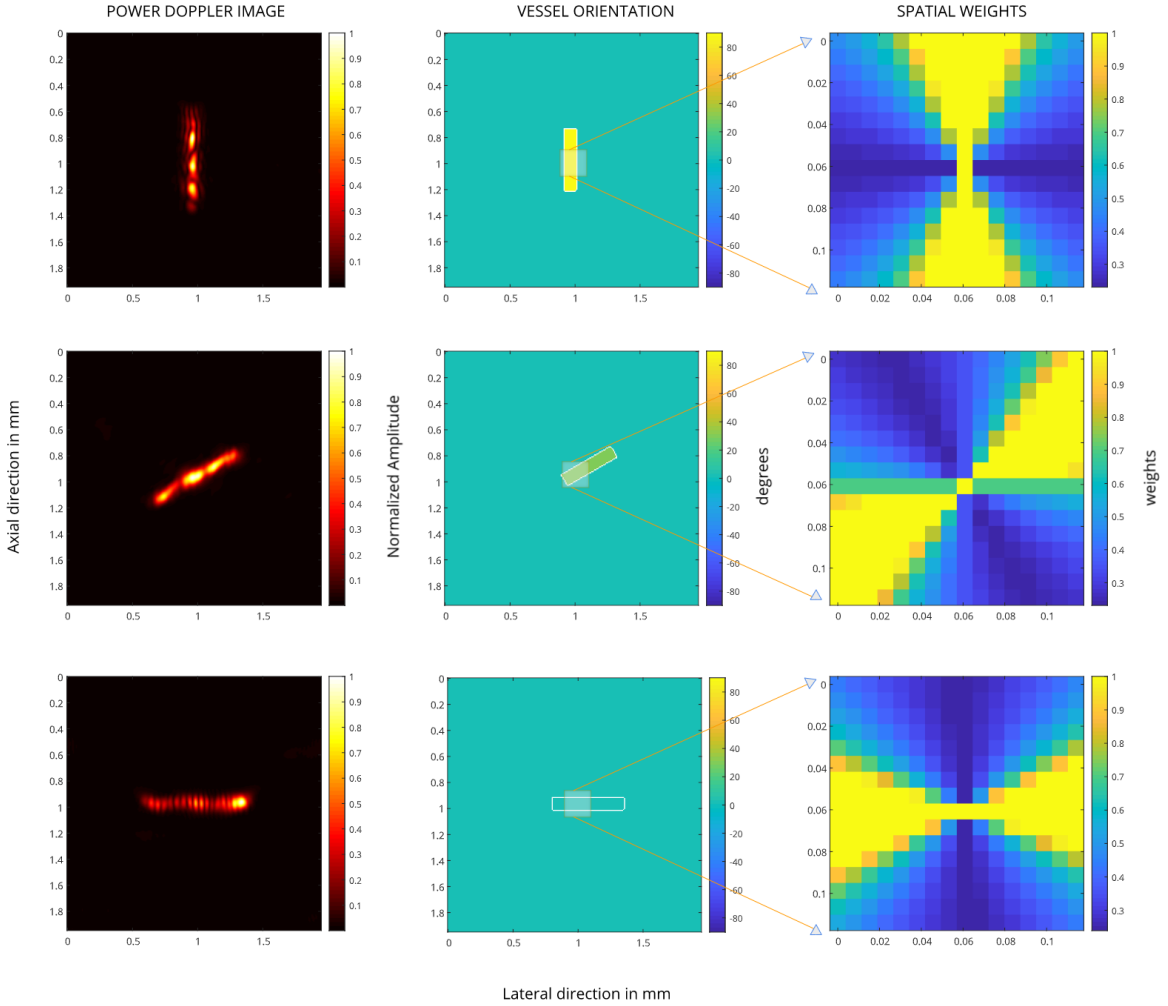

Figure 4.2: The spatial weights computation from the PDI. The first column shows the PDI for the three versions in the spatial domain. The second column shows the respective orientations of the vessels in degrees and the third column shows the distribution of the spatial weights (Huber function with p = 1.5 and s = 1/16) for the selected block (highlighted by the orange marker) in the second column.

4.2.3 Frame-wise Velocity Estimates

The velocity components are estimated using GOMP and the vectors are visualised at each pixel in the scanning region in Figure 4.3 and Figure 4.4. The vectors visualized at a specific frame number correspond to the frame-wise estimates after considering

four filtered frame pairs ($n_{avg} = 4$). The total number of frames for which frame-wise estimates are calculated after using n_{avg} frame pairs is

$$frames = \frac{N_{ensemble} - 2}{n_{avg}}. \tag{4.1}$$

In these figures, the frame-wise estimates are shown at different frames which shows the velocity estimation at different acquisition times. The pixel of the image shows the magnitude of the velocity and the arrows over the image point towards the direction of the flow. The length of the arrow is directly proportional to the velocity magnitude.

The frame-wise velocity vectors that are measured using Normalized Cross-Correlation are shown in Figure 4.3. Here, the first row contains the ground truth representation of actual velocities and the rows afterward show the vector visualization for three distinct frames. The columns contain the estimates for each of the versions. In the vertical vessel simulation, the NCC vectors are mainly biased towards the positive axial and positive lateral directions. For the slanted vessel simulation, some of the vectors are aligned with the positive lateral direction while the majority of the other vectors are found within the vessel's periphery. With the visual inspection of the horizontal vessel simulation, it is observed that the direction of the estimated vectors is along the orientation of the vessel.

The frame-wise vector visualization for the proposed method is shown in a similar format as shown for the NCC method in Figure 4.4. The directivity of the vectors is considerably improved in the vertical vessel simulation. In the slanted version, the vectors which were aligned to the horizontal direction in the NCC methodology are now aligned along the vessel's orientation and the vectors in the horizontal vessel simulation are completely aligned along the horizontal direction.

All the velocity measurements across the 60 filtered, compounded frames are displayed as scatter plots with the y-axis indicating the measured axial velocity and x-axis indicating the measured lateral velocity components. The color of the plot markers correspond to the Pearson Correlation Coefficient (PCC) calculated for the matched block pairs of consecutive frames. In Figures 4.5, 4.5 and 4.5, the direction of the estimates found using the proposed method is closer to the actual direction (indicated by a solid black line in the scatter plot) when compared to the velocity estimates found by the NCC method. The higher PCC values for the scatter points in Figure 4.5 are farther away compared to the lower PCC values in both the speckle tracking methods. All the measurements by the proposed method in the slanted vessel are below the actual velocity. The actual velocity is indicated by a solid black circular marker in all the scatter plots.

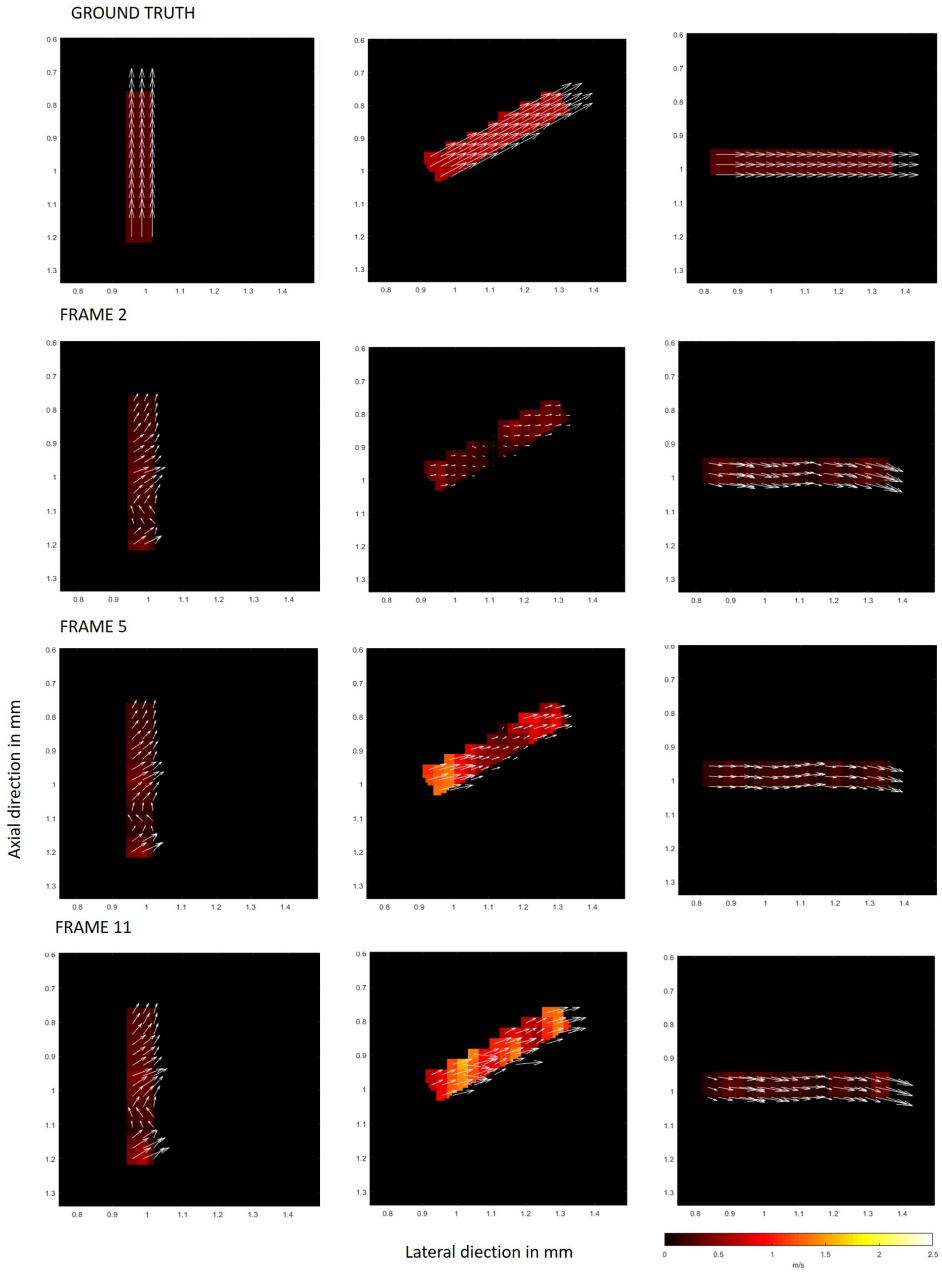

Figure 4.3: The frame-wise vector visualization for the three different time stamps at each spatial location of the simulated vessels. The first column shows the velocity vectors for the vertical vessel, the second column for the slanted vessel and the third column for the horizontal vessel. The velocity magnitude of the ground truth is displayed by the hot color map and the velocity direction of the ground truth is pointed with the arrows. The first row shows the ground truth for the three versions and the consecutive rows show the NCC measured vectors per frame. The spurious flow directions are observed in the vertical vessel simulation; high magnitude velocity vectors are obtained in the slanted vessel simulation; and the velocity vectors within the vessel are found in the horizontal vessel simulation.

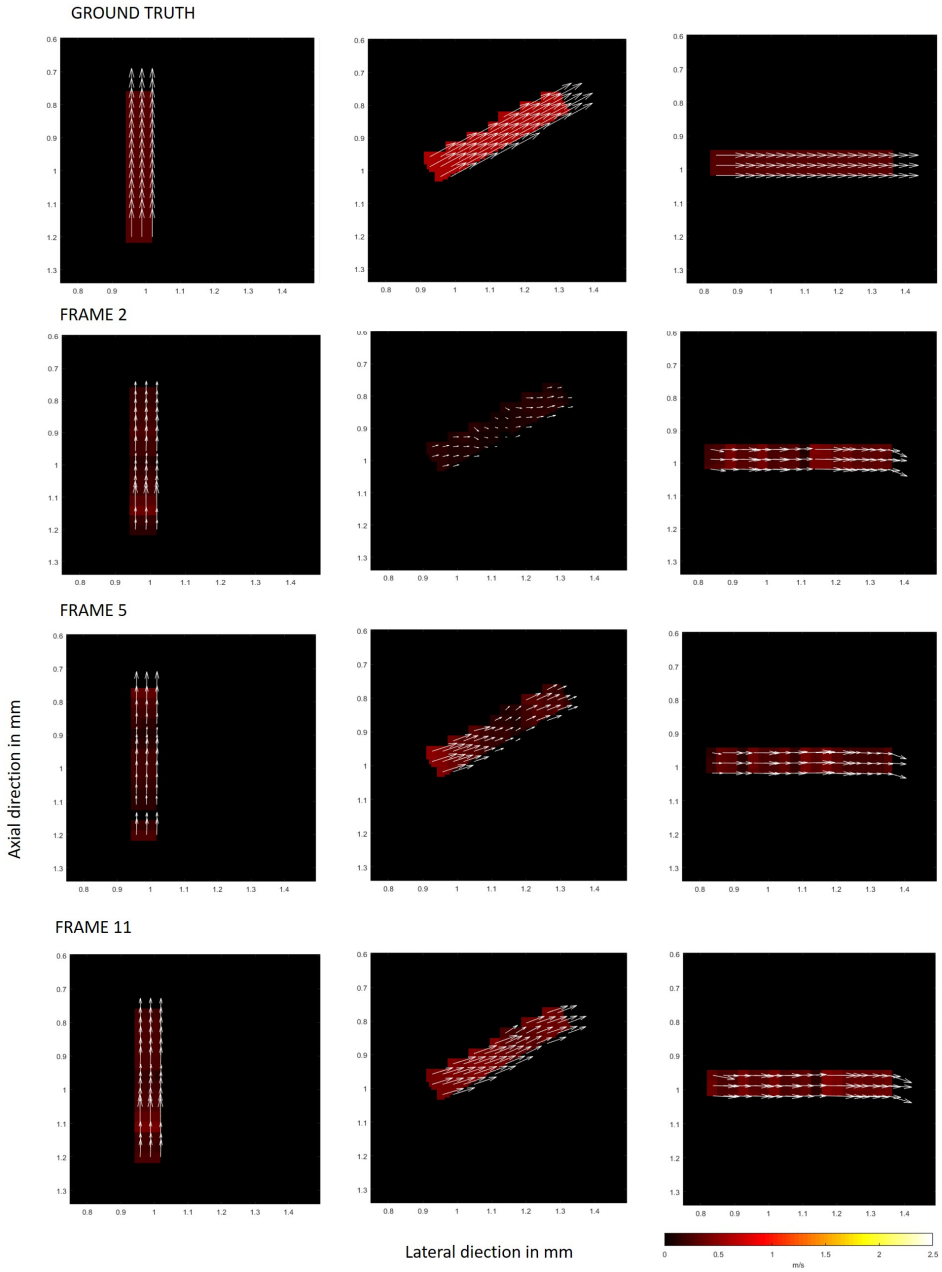

Figure 4.4: The frame-wise vector visualization for the three different time stamps at each spatial location of the simulated vessels. The first column shows the velocity vectors for the vertical vessel, the second column for the slanted vessel and the third column for the horizontal vessel. The velocity magnitude of the ground truth is displayed by the hot color map and the velocity direction of the ground truth is pointed with the arrows. The first row shows the ground truth for the three versions and the consecutive rows show the measured vectors per frame using the proposed method. Flow directions are obtained within the vessel's orientation and the measured magnitude values are lower than the ground truth.

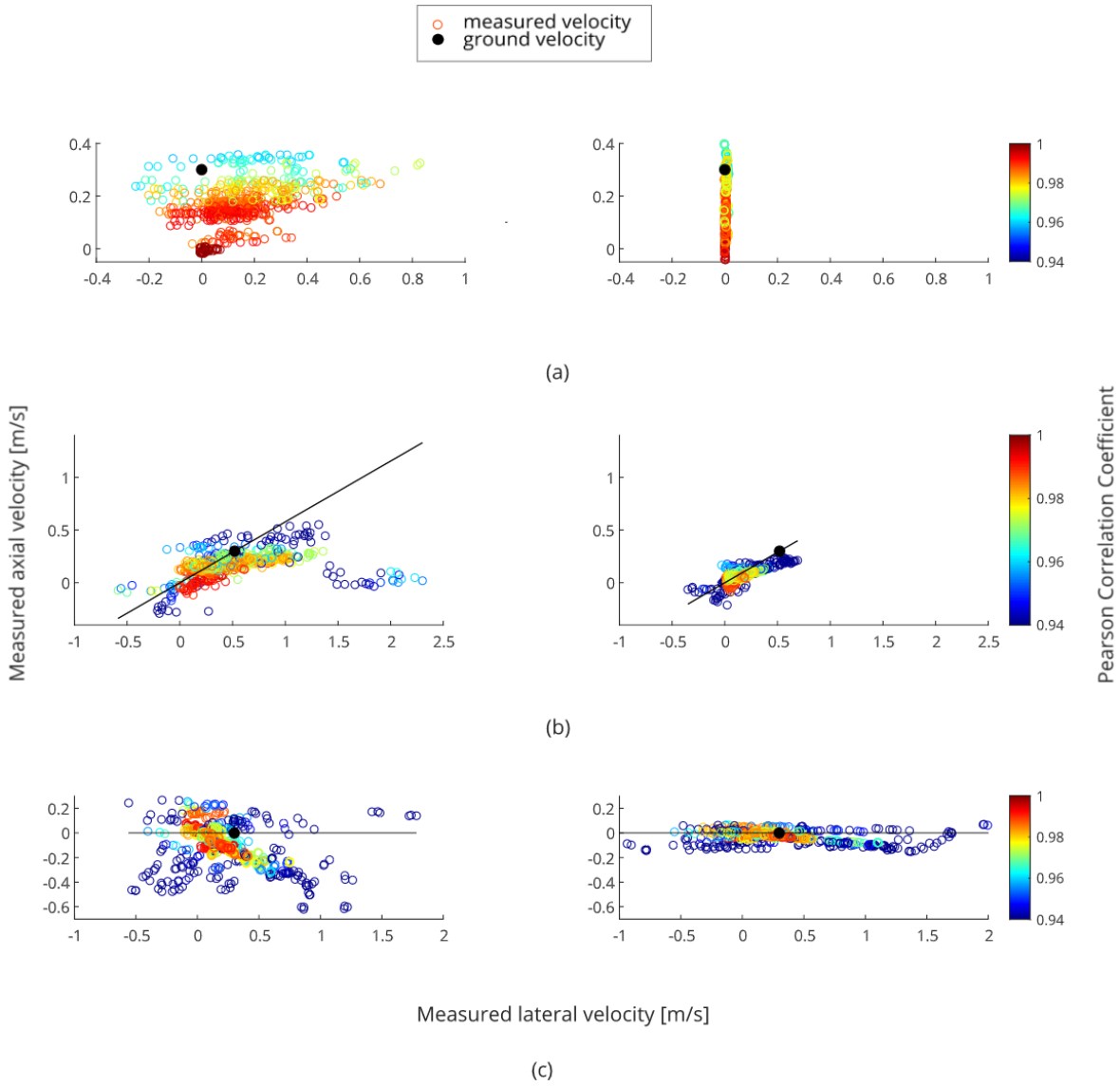

Figure 4.5: Scatter plots consisting of all the velocity measurements for the 60 filtered, compounded frames. The first column shows the scatter plots for the NCC method and the second column shows the scatter plots for the proposed method. The measurements are marked according to the Pearson Correlation Coefficients. (a) compares the measurements of the vertical vessel, (b) of the slanted vessel and (c) of the horizontal vessel. The actual velocity is shown by a solid black disc and the flow direction is indicated by a solid black line. The variance of the measurements is reduced and the measurements are aggregated along the direction of the actual velocity.

4.2.4 Final Velocity Estimates

The final velocity estimate is given by computing the mean of all the velocity measurements at each spatial position over the ensemble length. The measurements which are more than three standard deviations away from the mean are removed to compute the regression and performance parameters. The linear regression parameters like the mean (μ), standard deviation (σ) and Mean Square Error (MSE) are calculated to further investigate the performance of the estimators [21]. The regression values are calculated individually for the lateral and axial components of the velocity vector as seen in Table 4.3. The table lists the values for the two speckle tracking techniques i.e. NCC and the proposed method. The σ is less for the proposed method. The difference in the performance among the three simulated versions is further investigated in Chapter 5.

TABLE 4.3. LINEAR REGRESSION ANALYSIS OF THE AXIAL AND LATERAL VELOCITY COMPONENTS AS ESTIMATED BY NCC AND GOMP

Versions	Velocity	NCC			GOMP		
		μ	σ	MSE	μ	σ	MSE
Vertical	Axial	0.17	0.08	0.02	0.20	0.10	0.01
	Lateral	0.15	0.16	0.04	$\sim$0	$\sim$0	$\sim$0
Slanted	Axial	0.17	0.10	0.02	0.08	0.05	0.04
	Lateral	0.47	0.36	0.13	0.17	0.13	0.13
Horizontal	Axial	-0.08	0.14	0.02	-0.02	0.04	$\sim$0
	Lateral	0.16	0.21	0.06	0.24	0.32	0.10
Total			1.07	0.29		0.65	0.28

The final velocity estimates for the new technique are shown in Figures 4.6, 4.7 and 4.8 showing the vertical, slanted and horizontal versions respectively. Each figure pictorially represents the mean axial velocity, mean lateral velocity, mean velocity magnitude and mean velocity direction over the ensemble length. The mean is computed at a given pixel for the frame-wise estimates obtained during the ensemble length acquisition. The mean velocity magnitude is the value computed using the mean axial velocity and mean lateral velocity at each pixel. Similarly, the mean velocity direction is computed using the mean values of the components at each pixel.

In Figure 4.6, the mean axial component is uniform and close to the actual axial velocity component of 0.3m/s; and the mean lateral component is around the actual magnitude of 0m/s at each spatial location. These mean components set the mean direction of the velocity vectors to be in the perpendicular direction to the scanning region. The mean direction of the vertical vessel simulation is comparable to the ground truth. The slanted vessel simulation results are in Figure 4.7. It shows that both the axial and lateral components are under-estimated values of the actual velocity components. The mean direction of velocity flow is nearly 10° less than the actual direction of 30°. In Figure 4.8, the mean velocity magnitude is approximately equal to the mean horizontal velocity as the mean vertical velocity component is almost equal to 0m/s. The mean magnitude of the horizontal vessel is around the actual velocity magnitude of 0.3m/s.

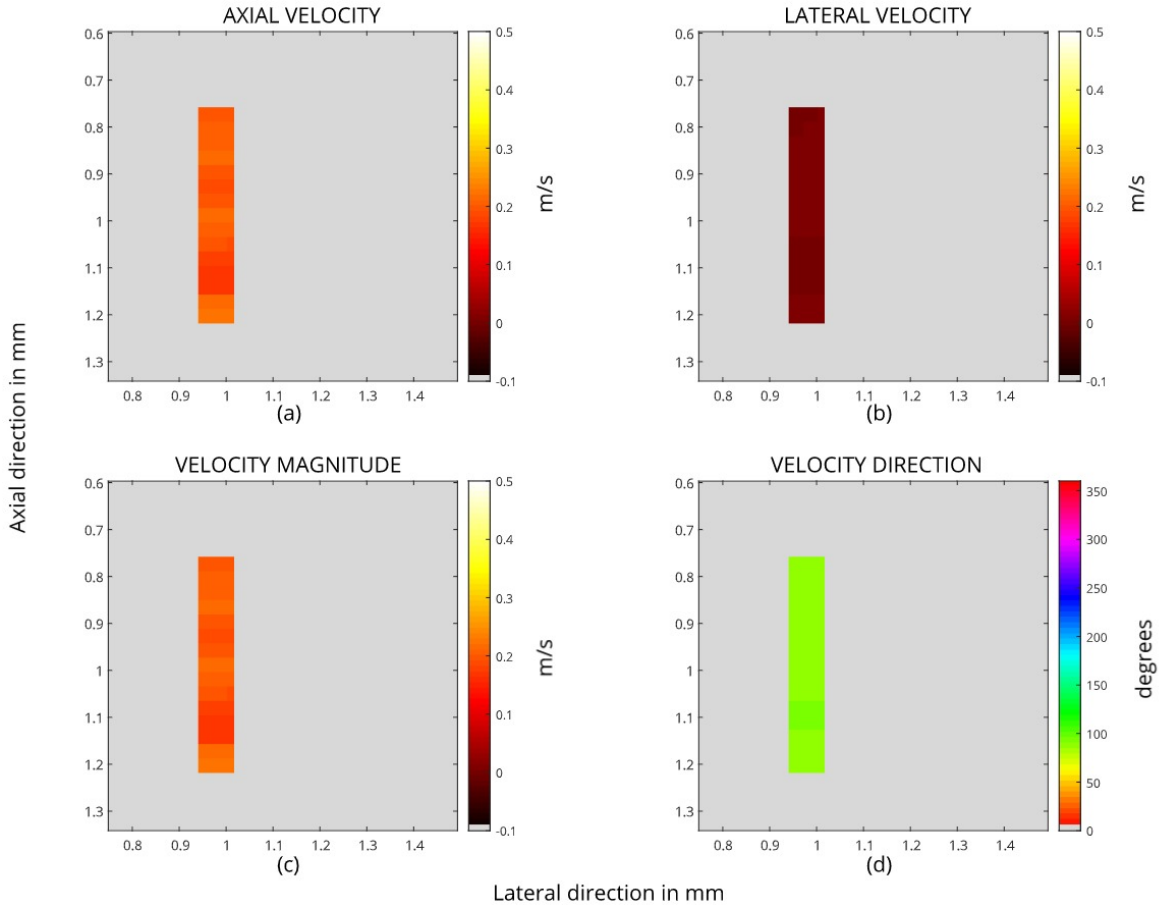

Figure 4.6: Final velocity estimates for the vertical vessel. The mean of the pixel measurements is computed to obtain the final estimates. The velocity magnitude in (c) and velocity direction in (d) are calculated from the mean axial velocity (a) and the mean lateral velocity (b) components. The measured axial and lateral estimates resemble the actual velocity components. The actual vertical and lateral velocity is 0.3m/s and 0m/s respectively.

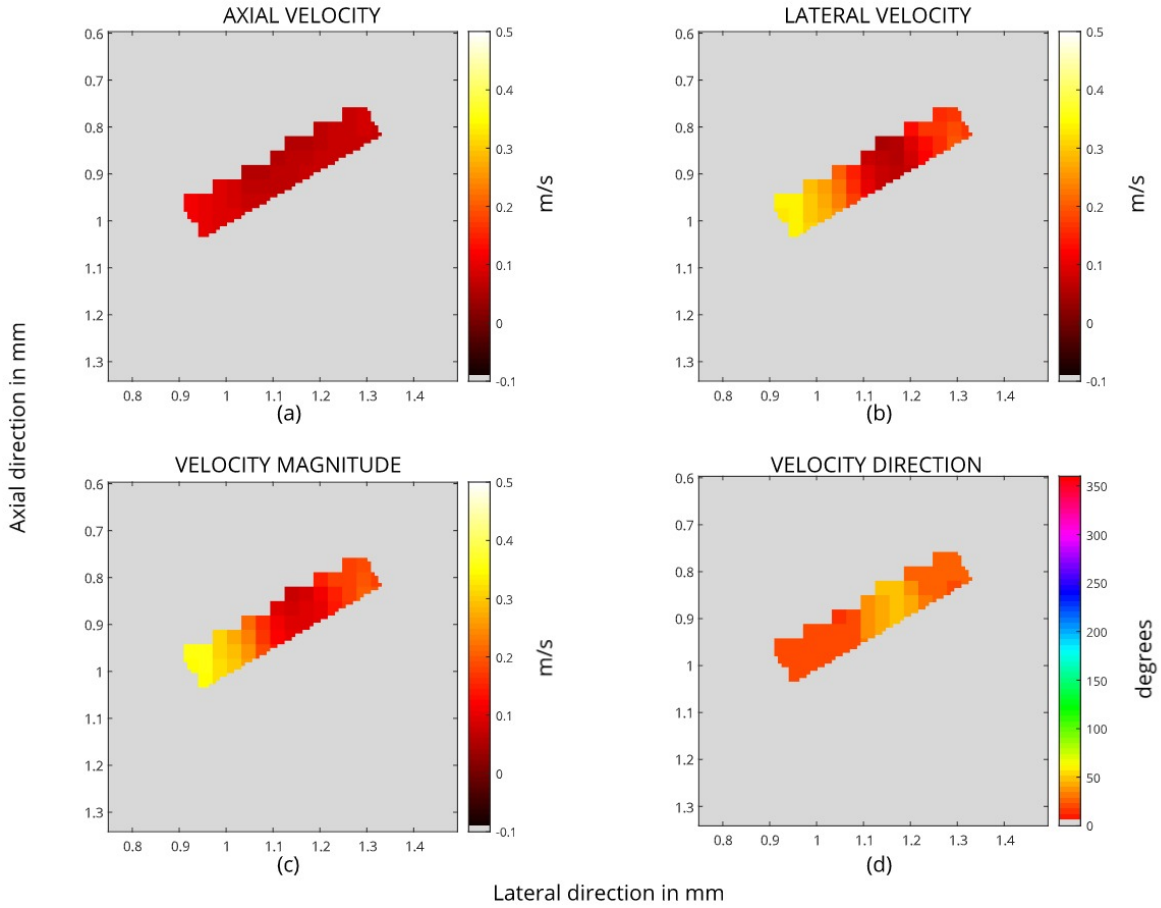

Figure 4.7: Final velocity estimates for the slanted vessel. The mean of the pixel measurements is computed to obtain the final estimates. The velocity magnitude in (c) and velocity direction in (d) are calculated from the mean axial velocity (a) and the mean lateral velocity (b) components. The measured axial and lateral components underestimate the actual velocity components. The actual vertical and lateral velocity is 0.3m/s and 0.5192m/s respectively.

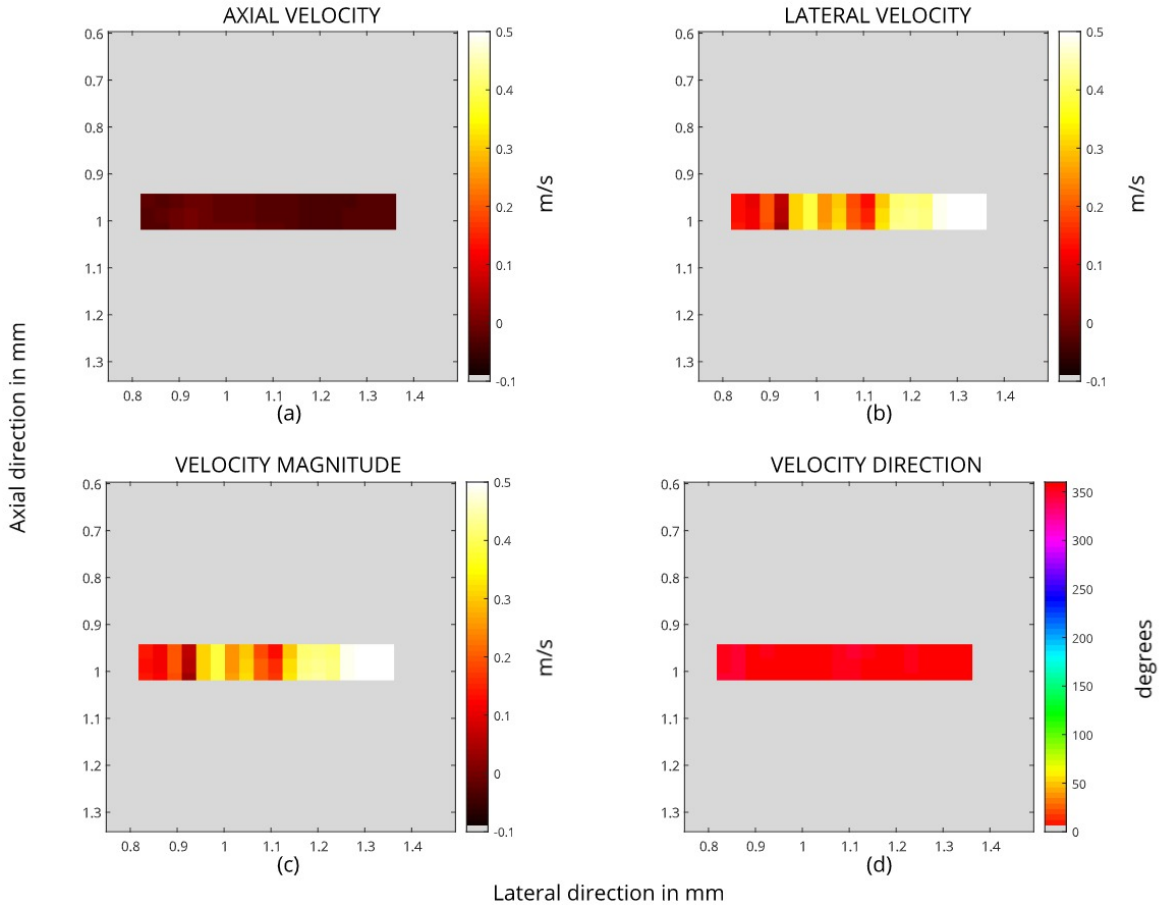

Figure 4.8: Final velocity estimates for the horizontal vessel. The mean of the pixel measurements is computed to obtain the final estimates. The velocity magnitude in (c) and velocity direction in (d) are calculated from the mean axial velocity (a) and the mean lateral velocity (b) components. The measured axial estimates resemble the actual axial velocity components but it shows variations throughout the length of the vessel. The actual vertical and lateral velocity is 0m/s and 0.3m/s respectively.

4.2.5 Performance Analysis

The performance of the velocity estimation techniques i.e. the NCC method and the GOMP method is compared based on the Mean Deviation (MD) and Mean Square Error (MSE). MD is the mean difference between the actual velocity component and the measured velocity component of each spatial position in the vessel. MD is computed at each frame and is represented in percentage by dividing the mean deviation by the maximum of the velocity component measured in the given frame. MSE for a given frame is calculated by taking the mean of the squared error between the actual velocity component and all the velocities measured before and till the given frame. The MD and MSE curves are plotted against the time of acquisition of the filtered, compounded frames.

The performance plots for all the versions are shown in Figures 4.9, 4.10 and 4.11. Due to the underestimation of the measurement values, the performance of GOMP is poor in the slanted vessel simulation whereas MSE for the horizontal and vertical vessel is better for GOMP than NCC.

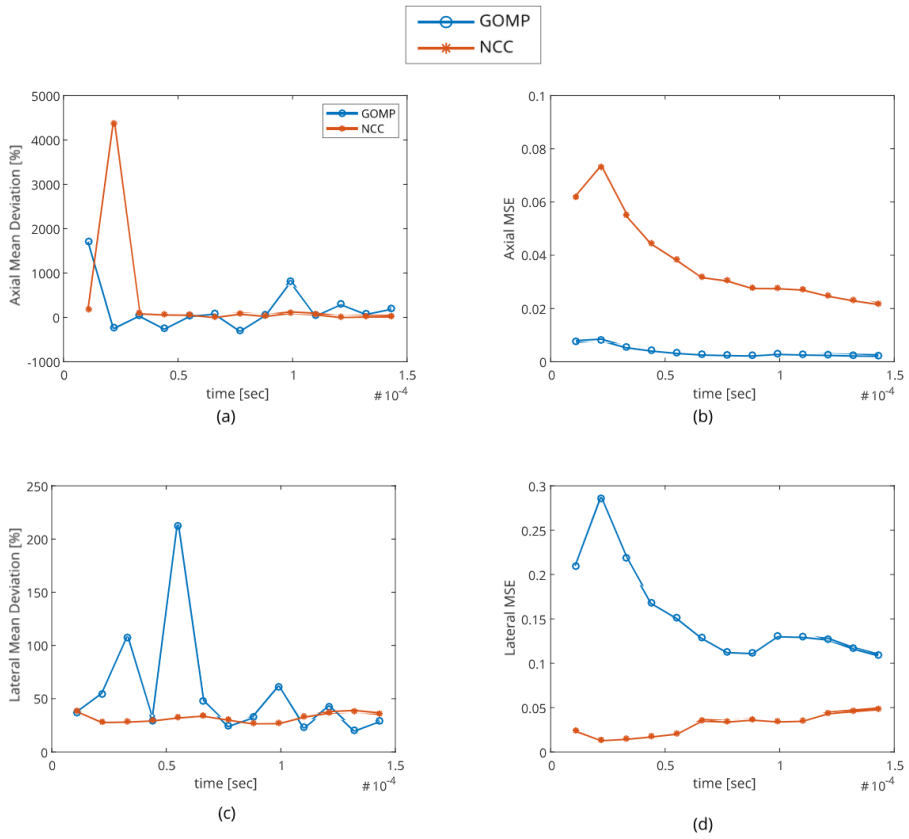

Figure 4.9: Performance Comparison between the NCC and GOMP methods for the vertical vessel simulation. (a, b) show the MD and MSE for the axial direction; (c, d) show the MD and MSE in the lateral direction. The axial MD and MSE for the GOMP method is lower than the NCC. The lateral component has higher MAD but has lower MSE than NCC. The measurements of the lateral components varies within a large range but the limits of the range are close to the actual axial components.

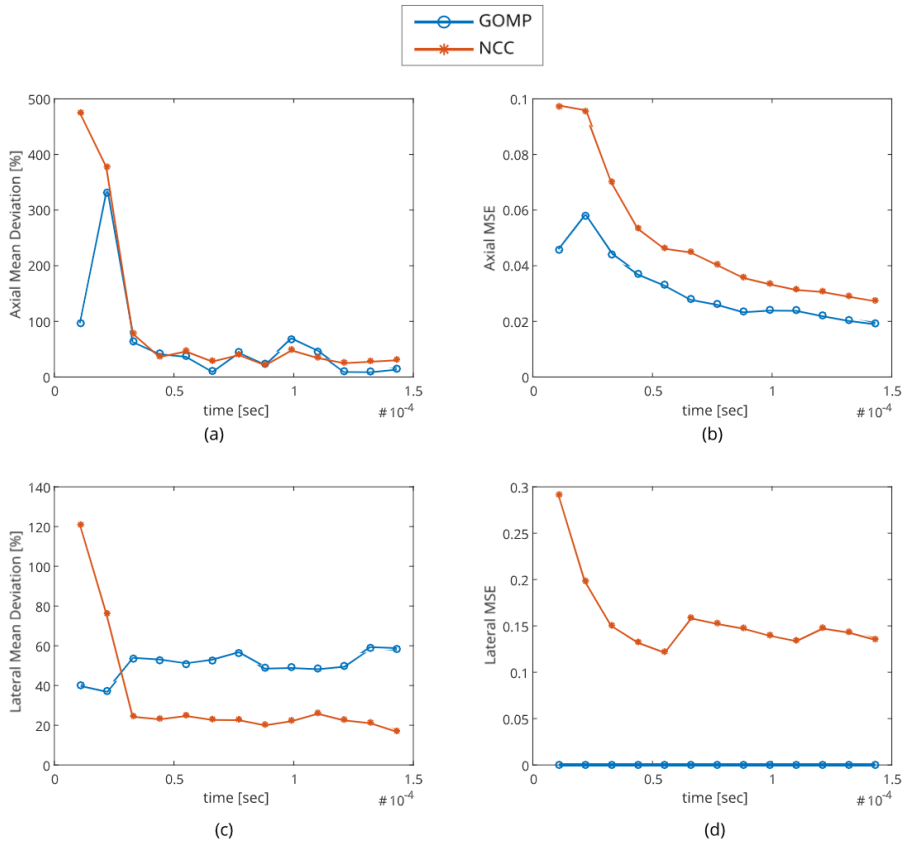

Figure 4.10: Performance Comparison between the NCC and GOMP methods for the slanted vessel simulation. (a, b) show the MD and MSE in the axial direction; (c, d) show the MD and MSE in the lateral direction. The MD and MSE for the GOMP method is more for both the axial and lateral velocity components because underestimation of the actual velocity components takes place with the application of a directional constraint.

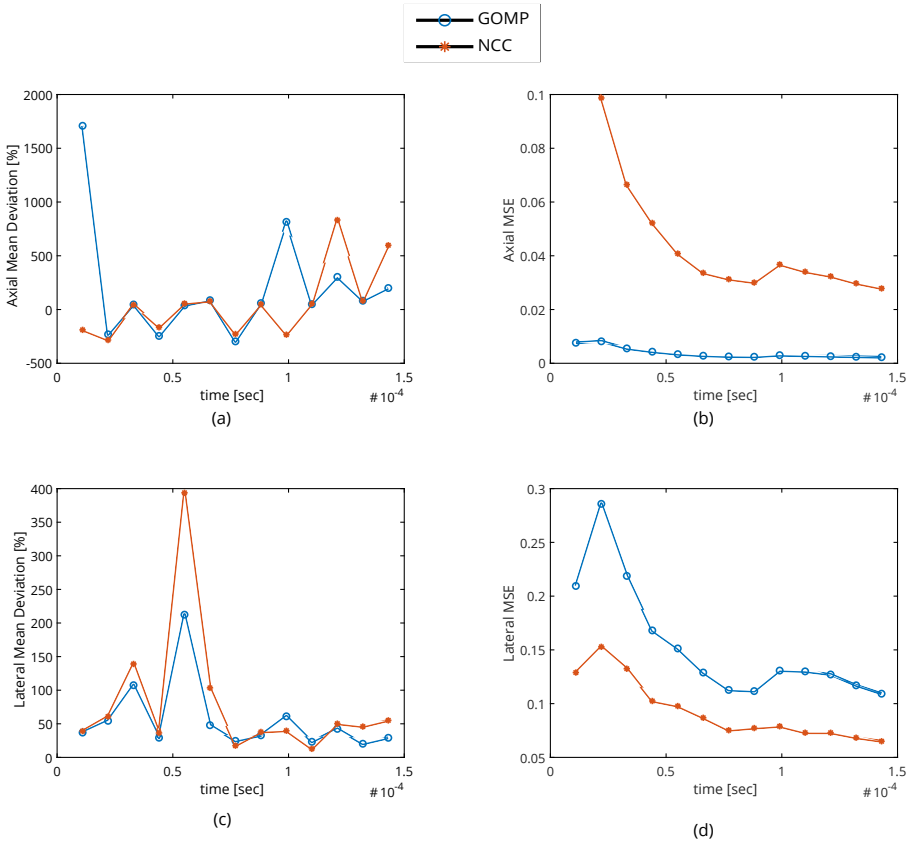

Figure 4.11: Performance Comparison between the NCC and the GOMP methods for the horizontal vessel simulation. (a, b) show the MD and MSE in the axial direction; (c, d) show the MD and MSE in the lateral direction. The MD is similar for both the components but the MSE has a lower value than NCC.

4.3 In Vivo Results

The new approach is applied on the cerebellum region of the mouse brain to estimate the velocity vectors. The orientation of the vessels needs to be calculated for the implementation of this approach. With the usage of the angle detection technique as explained in Chapter 3, the orientation of the vascular network is obtained from the PDI of mouse brain is shown in Figure 4.12.

The n_{avg} to find the velocity vectors using GOMP in the *in vivo* data-set is also 4. The other important details for the ultrasound setup are given in Table 4.4. The block size of 16 $\times$ 16 pixels is used for the speckle tracking. This size ensures that the speckle pattern in the local region is completely contained inside this block area. The size is enough to capture the movement of speckles within one vessel and avoid the movement of speckles moving in different directions.

The frame-wise representation of the velocity estimates by the proposed and the NCC methods on this data-set is shown in Figure 4.13 and 4.14, respectively. With the proposed method in Figure 4.13, some vessels show one flow direction in all the frames. From (4.1), the total number of frames available for the computation of frame-

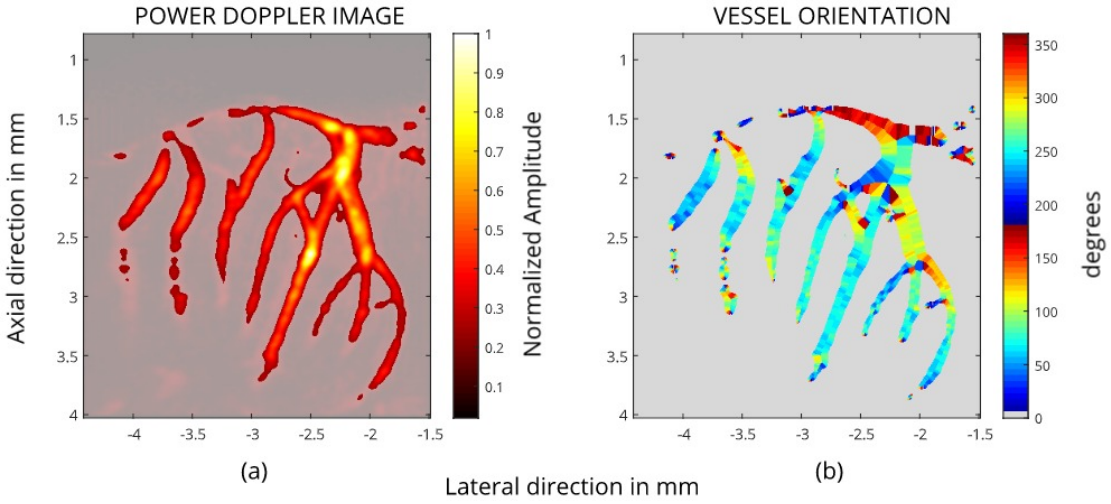

Figure 4.12: Illustration of the vessel's orientation computed from the Power Doppler Image (PDI). (a) the PDI is shown and (b) the orientation of the vessels at each pixel is shown. The data-set is of the cerebellum region of the mouse brain.

TABLE 4.4. THE PARAMETERS OF THE ULTRASOUND SETUP FOR THE *IN-VIVO* EXPERIMENT

In-Vivo Ultrasound Setup			
Central Frequency	25MHz	Frame Frequency	600Hz
Pitch	0.069 mm	Ensemble frames	200
Kerf	0.020 mm	Number of angled emissions	20
Pixel resolution	$[\lambda/8, \lambda/8]$	Angles Range	$[-5°, 5°]$
Number of elements	256	Angle Increment	0.5263°
High Pass Filter	Butterworth	Cut-off frequency	60 Hz
Apodization Kernel	Smoothed Square	Total Acquisition time	0.3333 s

wise estimates is 48. In other vessels, there are regions within the same vessel showing the flow in opposite direction to the majority of the flow in the vessel. There are even alternating flow directions at the same spatial position across the frames. It is assumed that the flow within a vessel should have same direction through out the ensemble acquisition. From these observations, it could be concluded that the tracking of the real signature of the filtered frames gives faulty estimates for displacement of the scatterers in particular directions. When the frame-wise vectors of the proposed method are compared with the NCC method, it is observed that the NCC velocity estimates do not provide true flow as shown in Figure 4.14.

With the increasing number of frames, the frame-wise velocity estimates are averaged till the given frame number is shown in Figure 4.15. In comparison with the frame-wise estimates shown in Figure 4.13, the averaged frame-wise estimates follow a consistent flow direction.

The complete overview of the final velocity estimates is given in Figure 4.16 that displays the mean axial velocity, mean vertical velocity, mean velocity magnitude and

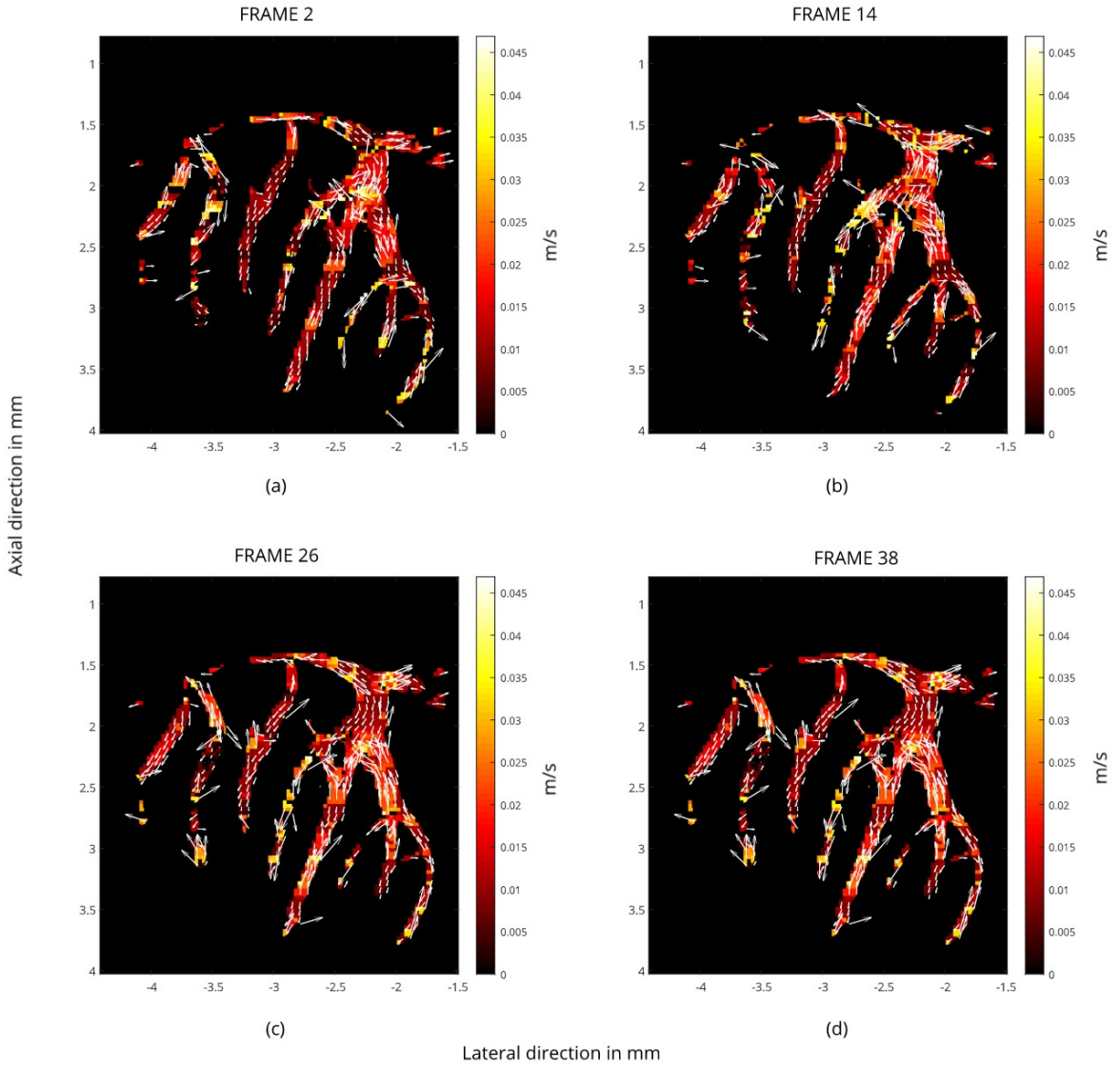

Figure 4.13: The frame-wise vector visualization across four time stamps. The arrows point in the velocity direction and intensity of the map indicate the velocity magnitude measured by the proposed method. The length of the arrow is directly proportional to the velocity magnitude.

the mean direction in its four sub-figures configuration. From the Figure 4.16, the signs of the axial and lateral velocity components are such that the flow direction is ensured within the vessel's curvature.

In the mean magnitude velocity plot, certain regions within the same vessel have higher magnitude than the rest. In the mean direction plot, it is easy to identify the regions where the frame-wise vectors show different flow directions at the same spatial positions because the mean direction is not within the vessel's curvature. These fluctuating flows can be detected by computing the variance of the estimated direction of the frame-wise velocity estimates. The pixels which have low directional variance

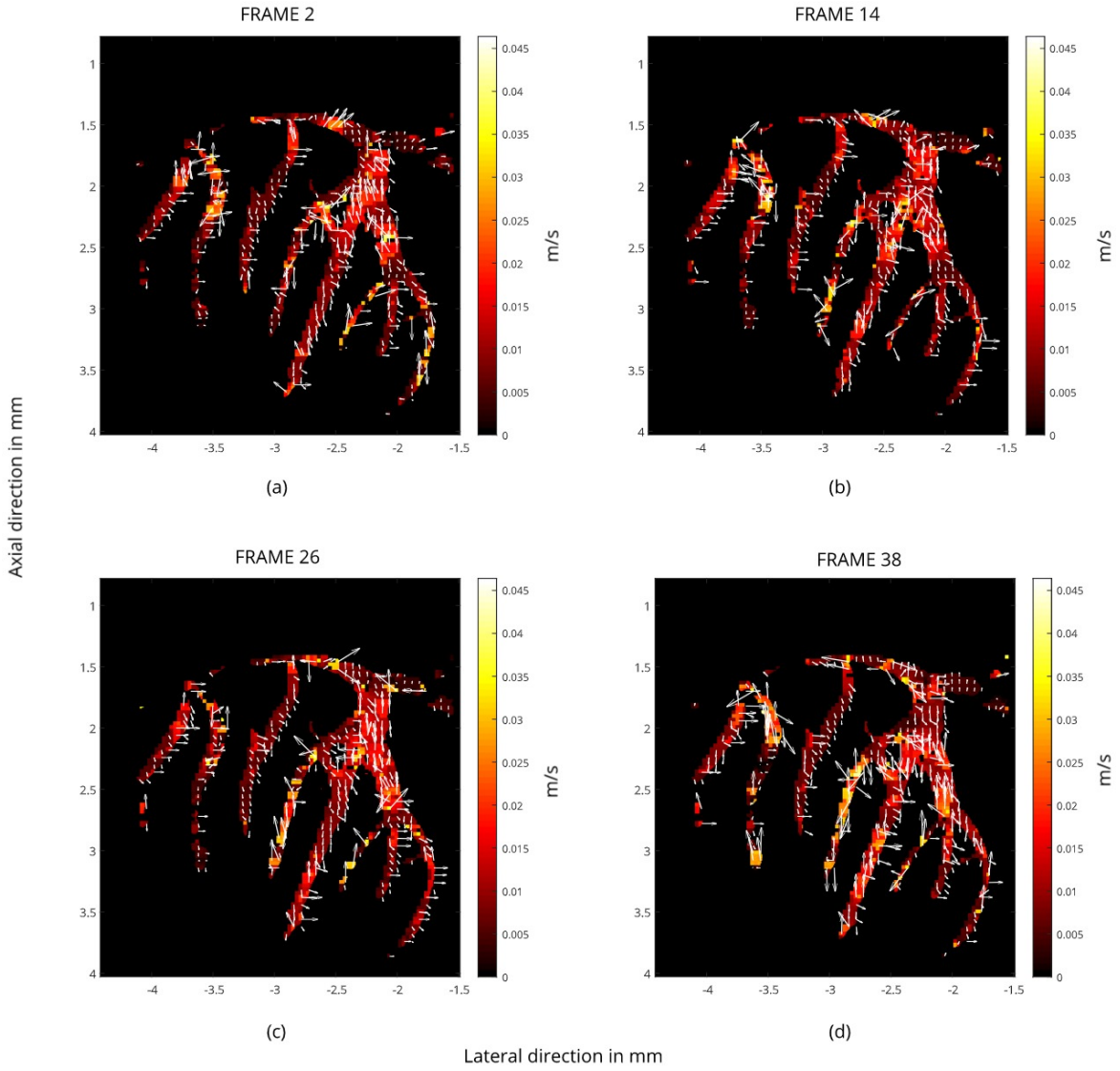

Figure 4.14: The frame-wise vector visualization across four time stamps. The arrows point in the velocity direction and intensity of the map indicate the velocity magnitude measured by NCC. The length of the arrow is directly proportional to the velocity magnitude. The blood flow is not observed within the vessel's curvature but in random directions.

also have high mean PCC as shown in Figure 4.17. The mean PCC of each pixel is computed on the PCC values of the frame-wise velocity estimates.

In Figure 4.18, the Doppler velocities in the cerebellum region and the Pearson Correlation Coefficient map are shown. For the proposed method, it can be seen that the estimated flow direction of the regions have the same direction as that of the Doppler flow estimates with high mean PCC. The portion of the vessels which show positive Doppler estimates also show positive axial GOMP estimates. There are some regions which have contradiction between the estimates of the Doppler and the proposed method.

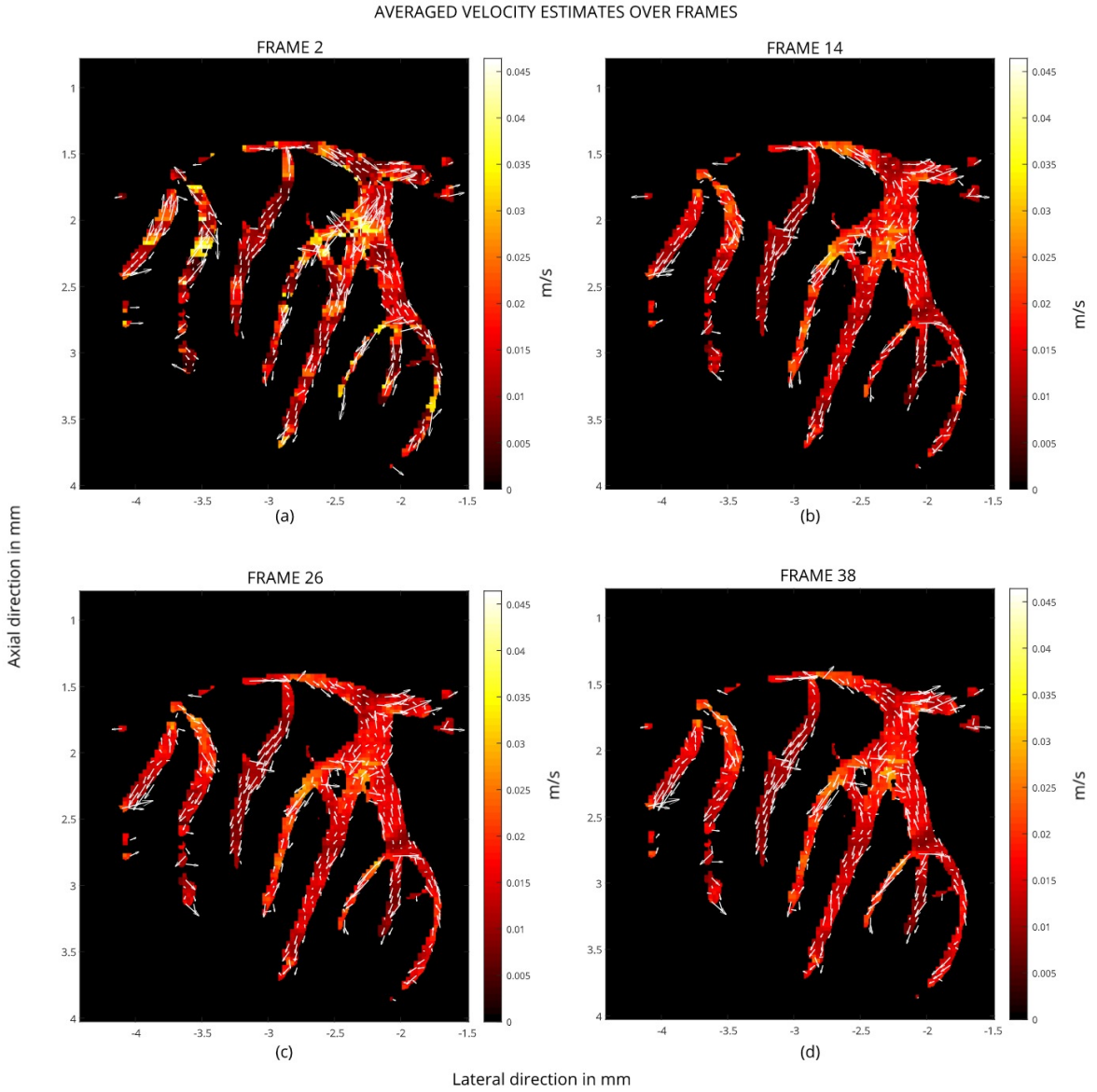

Figure 4.15: The averaged frame-wise velocity estimation till the given frame. The arrows point in the velocity direction and intensity of the map indicate the averaged velocity magnitude measured by the proposed method. The length of the arrow is directly proportional to the velocity magnitude.

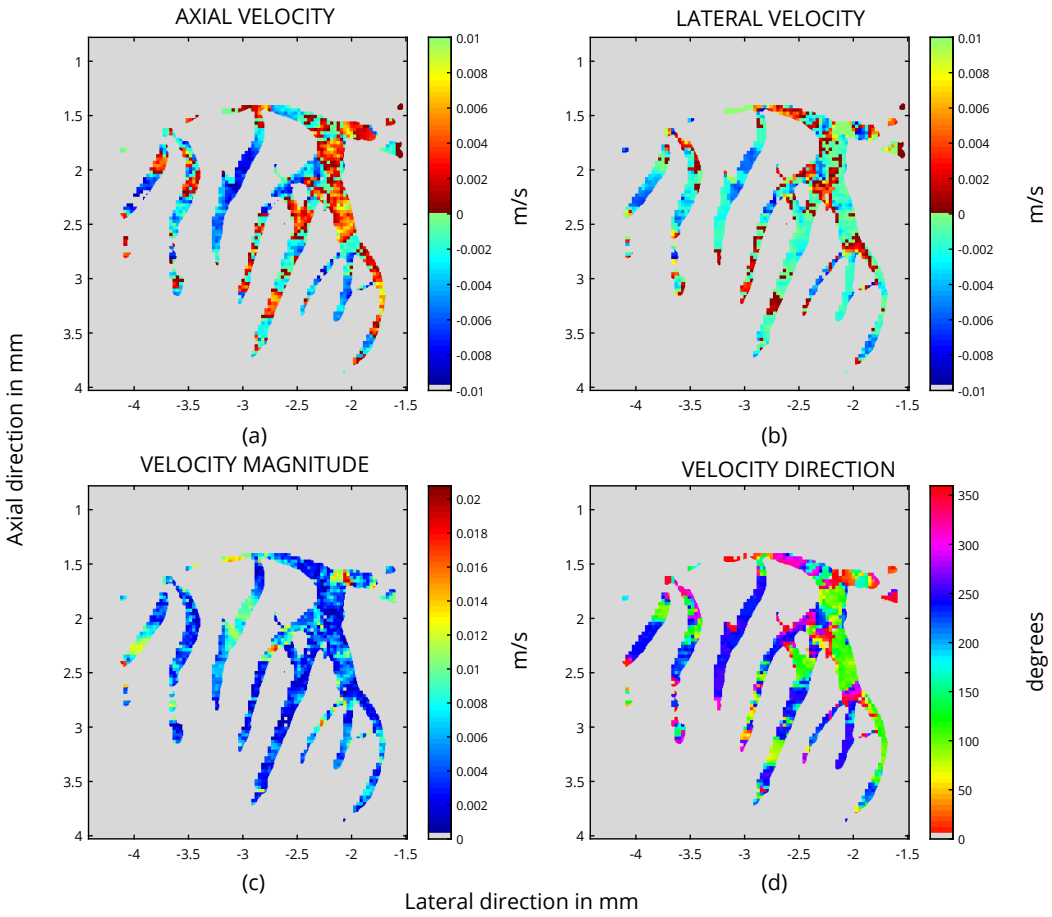

Figure 4.16: Final velocity estimates computed using the proposed method for the *in vivo* experiment. The final estimates are the mean of the measurements obtained at each pixel. The final velocity magnitude and velocity direction is calculated using the mean of the lateral and axial components. (a) is the mean axial velocity and (b) is the mean lateral velocity component at each pixel in the vessel. (c) shows the final velocity magnitude computed from the mean of the individual components and (d) shows the direction of the final velocity estimate.

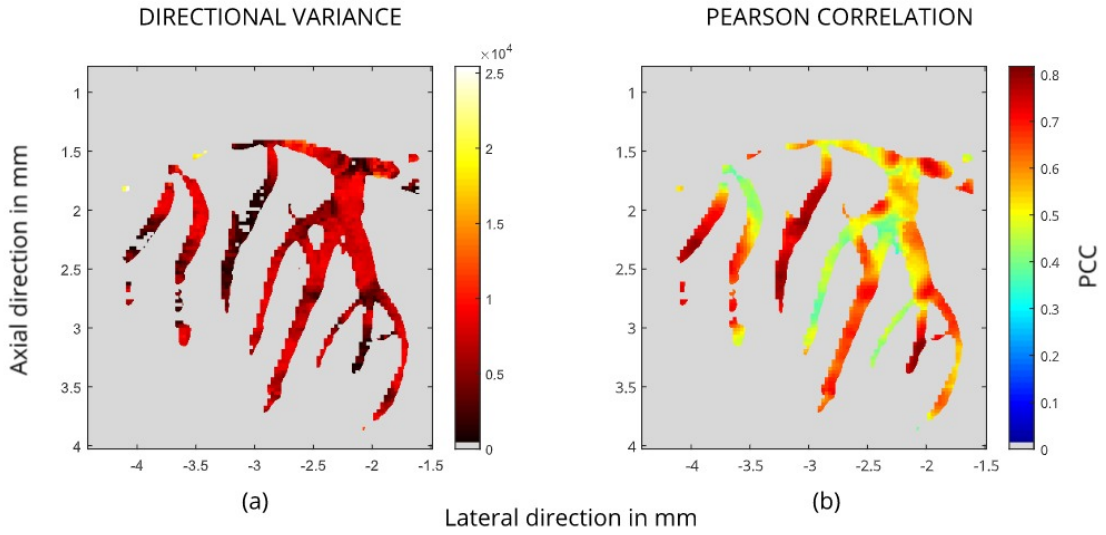

Figure 4.17: The variance of the estimated direction of the frame-wise velocity estimates is visualized in (a). High variance shows the estimated flow fluctuations at the given region. Low variance shows the stability of the estimated flow by the proposed method. The stable regions are further supported with high mean PCC as shown in (b).

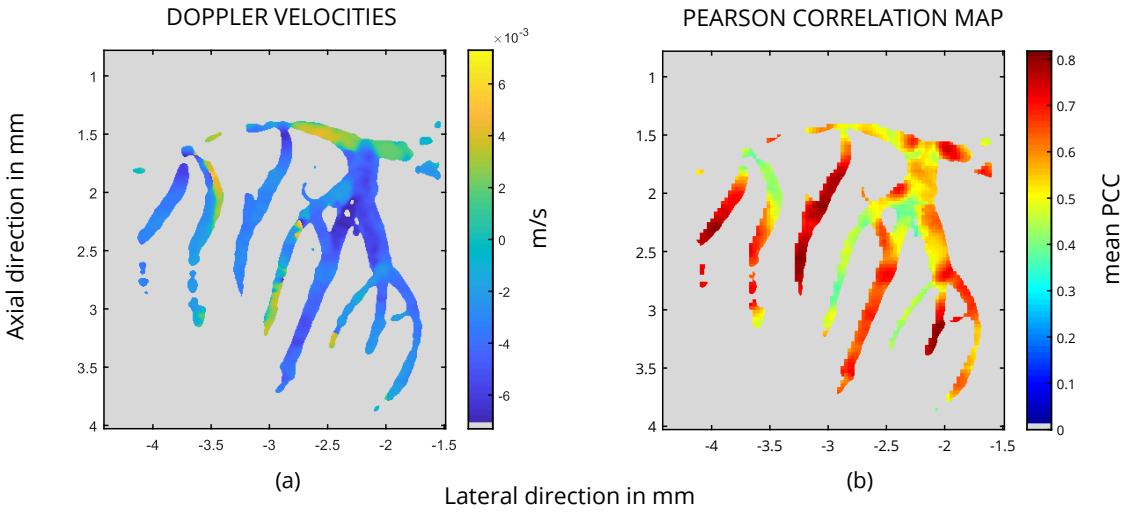

Figure 4.18: Velocity estimation in the cerebellum of the mouse brain using the Doppler method is shown in (a). The mean of Pearson Correlation Coefficients (PCC) is computed for the best match provided by GOMP at each pixel as in (b). It is observed that the high correlated GOMP values also satisfy the flow directions provided by the Doppler estimates.

5 Discussions and Future Work

Blood velocity estimation for Ultrafast Ultrasound in the brain vessels is performed using the speckle tracking technique. The standard method for speckle tracking is NCC. This method when applied to the fine vascular network of the brain provides spurious velocity directions. The proposed method for speckle tracking uses prior information in the form of the vessel's orientation to estimate the velocity magnitudes along the curvature of the vessel.

Section 4.2 compares the NCC method to the proposed method on a simulated dataset obtained using the k-Wave toolbox in MATLAB. The methods are compared using the parameters of linear regression analysis that include mean (μ), standard deviation (σ) and Mean Square Error (MSE). The combined linear regression analysis for the three simulated versions is that velocity estimates of the proposed method have 38% less standard deviation and almost the same MSE as the NCC method. This is due to the application of a directional constraint which aligns all the measurements along the direction of actual velocities.

The proposed method provides a mathematical framework on which different constraints can be applied to regularize the resultant flow. In this thesis, velocity is estimated by using a directional constraint. This is accomplished by weighing the columns of the dictionary in the system model using the spatial weights. Spatial weights are used as prior constraint to find shifts between two frames using the GOMP. The matching pursuit works through one iteration that finds one column index of the dictionary. It would be expected that with the increasing number of iterations, the new selected column index of the dictionary that corresponds to a new shift would be near to the previously calculated shift values. In this case, a method to interpret the resultant shift from the selected indices should be developed in future.

Speckle tracking is carried out on the real signature of the filtered, compounded frames. This thesis, explores the speckle tracking in the domain of the real signature which has not been studied before. As the speckles are to be tracked in the narrow vessels, the absolute signature of the filtered, compounded frames is not used as it gives a smooth speckle pattern making it difficult to track the speckle movement. The interference pattern is granular for the real signature because of which the real values are used for velocity estimation.

Most of the velocity vectors estimated using NCC do not flow along the orientation of the vessel. Hence, there is a requirement to guide the estimation method to find the displacement within the vessel's orientation. The estimated vectors nicely align along the vessel when the directional constraint is enforced on the matching process using GOMP. As seen from the scatter plots in Figure 4.5, the variance of the velocity estimates measured by the proposed method has been reduced as the direction of the velocity estimates is concentrated along the orientation of the vessel.

The performance between the NCC and the GOMP methods is analyzed per frame

using Mean Deviation (MD) and MSE. The performance of these methods is tested on the three simulated versions consisting vessels with different orientations. The k-Wave toolbox is used to create the simulation data-set for the fixed medium properties of the scanning region. Since the medium properties are known, MD and MSE can be calculated for the simulation data-set.

The MD per frame measured by GOMP is lower either in the lateral direction or the axial direction depending on the direction fixed for the actual velocities. The MD per frame captures the percentage of mean deviation of the measurements from the ground truth with respect to the maximum measurement in the frame. The MD plots in Figures 4.9, 4.10 and 4.11 are shown with respect to the time of acquisition of the frames. In the case of the vertical vessel simulation, the axial MD for GOMP is lower than the NCC and in the slanted vessel simulation, the MD in the axial and lateral directions is higher than the NCC. The MD results are influenced by the directional constraint, providing lower values when the measurements are around the actual velocity and higher values when the measurements are under-estimated.

The MSE for a given frame is the mean square of the error between the estimates and the ground truth. The mean of all the estimates until the given frame is used to compute the corresponding MSE for a given frame. The total MSE for the horizontal and the vertical vessels which is computed for the GOMP estimates is lower than the NCC. But, the MSE for the GOMP estimates is higher than NCC for the slanted vessel as all the measurements of GOMP are under-estimated.

The real signature of the filtered, compounded frames occur in the form of high and low sinusoidal waves that are alternately stacked. The resulting speckle pattern has higher discontinuity in the axial direction than in the lateral direction. The MSE of the proposed method is lower than NCC for the vertical vessel simulation and higher for the slanted vessel simulation. In the horizontal and slanted vessel simulation, the motion of the real speckle pattern between two frames is not well defined because the movement of Red Blood Cells (RBC) is in a direction where the speckle pattern is continuous. Hence, the shifts in the horizontal and slanted vessel simulation are not tracked with the required accuracy.

In the *in vivo* experiments, the Doppler velocity estimates show a downward blood flow motion in the cerebellum region of the mouse brain. The Doppler velocity estimation has been proven to have a higher sensitivity in the axial direction than in the lateral direction. The velocity vectors estimated by the proposed method show the motion of RBC in all the vessels. Some of the frame-wise estimates have high variance of the estimated flow direction and the others have consistent flow directions throughout the computation. The regions which have low variance in the estimated direction also have high mean PCC values. With the computation of variance, regions with consistent flow directions can be detected.

Moreover, the proposed method estimates are also compared with the Doppler estimates. As the Doppler method only computes the flow in axial direction, the axial flow of both the methods is compared. Most of the scanning region is in agreement with the flow directions estimated by both the methods but there are some regions where Doppler estimates have negative axial flow and the proposed estimates have positive axial flow. Aliasing of Doppler estimates could provide false flow direction. Due to

aliasing, it is observed that majority of the areas which have contradictory flow results have low negative Doppler velocities but high positive GOMP velocity estimates.

Future Work

The velocity vectors can be regularised in both the temporal and spatial domains as given in [1]. The temporal domain deals with the measurements at a given spatial position for the entire ensemble range, while the spatial domain deals with all the measurements in a particular slow-time stamp. The speckle tracking using GOMP has created a mathematical framework on which different types of constraints can be easily incorporated. In this thesis, a directional constraint is applied in the spatial domain to regularize the velocity estimates within the vessel's curvature. Even better velocity estimates might be found after the application of other spatial and temporal constraints.

In the proposed method, the final velocity estimates are provided per ensemble length. The velocity estimates for all the frames are averaged to compute the final velocity estimates. Instead of simple averaging, Kalman filtering can be adopted for the frame-wise velocity estimation that are measured by the proposed method. The state space model for Kalman filtering will depend on a constant flow model. The final velocity estimates would be the values provided by the Kalman filter at the end of the ensemble range. In this way, a minimum variance approach is adopted to enforce a constant flow profile at every time stamp between the present and past measurements in the ensemble range.

As discussed, the tracking of the real signature of the filtered, compounded frames is not much effective for the displacements inclined more towards the lateral direction. In the simulations, the actual displacement with respect to frame sampling frequency is small. The change in discontinuity of the real speckle pattern with increasing velocities could be studied to analyze the effectiveness of the proposed method.

6 Conclusions

The frame rate for ultrasound has increased with the development of the Ultrafast method. This has increased the focus on signal processing techniques to obtain reliable velocity estimates of Red Blood Cells flowing in the brain vessels. The velocity estimation of the blood flow in the brain is limited to the upward and downward directions with the standard ultrafast ultrasound acquisition procedure. Prior information in the form of vascular orientation is obtained by segmenting the Power Doppler Image. This information is incorporated using the Guided Orthogonal Matching Pursuit (GOMP) method for speckle tracking between frame pairs. When the GOMP method along with the directional constraint is applied on the acquired frames, velocity vectors are found within the vessel's curvature with a lower variance compared to the state-of-the-art Normalized Cross-Correlation (NCC) method [9].

A convergence analysis is performed to show that the Mean Square Error (MSE) of the velocity in the axial and lateral directions converge to a lower value in the proposed method compared to NCC. This is true for the horizontal and vertical vessels used for simulations. The MSE is higher compared to the NCC method for the slanted vessel simulation because the measurements are under-estimated and have low variance.

Although the new velocity estimator does not provide accurate magnitude estimates of the blood flow, it is a promising tool to provide a reliable direction in the fine vascular network of the brain.

Bibliography

[1] J. A. Jensen, S. I. Nikolov, A. C. Yu, and D. Garcia, "Ultrasound vector flow imagingpart i: Sequential systems," *IEEE Trans. Ultrason., Ferroelectr., Freq. Control*, vol. 63, no. 11, pp. 1704–1721, 2016.

[2] J. Richiardi, H. Eryilmaz, S. Schwartz, P. Vuilleumier, and D. Van De Ville, "Decoding brain states from fmri connectivity graphs," *Neuroimage*, vol. 56, no. 2, pp. 616–626, 2011.

[3] J. Bercoff, G. Montaldo, T. Loupas, D. Savery, F. Mézière, M. Fink, and M. Tanter, "Ultrafast compound doppler imaging: Providing full blood flow characterization," *IEEE transactions on ultrasonics, ferroelectrics, and frequency control*, vol. 58, no. 1, pp. 134–147, 2011.

[4] E. Macé, G. Montaldo, I. Cohen, M. Baulac, M. Fink, and M. Tanter, "Functional ultrasound imaging of the brain," *Nature methods*, vol. 8, no. 8, p. 662, 2011.

[5] G. Montaldo, M. Tanter, J. Bercoff, N. Benech, and M. Fink, "Coherent plane-wave compounding for very high frame rate ultrasonography and transient elastography," *IEEE transactions on ultrasonics, ferroelectrics, and frequency control*, vol. 56, no. 3, pp. 489–506, 2009.

[6] B. Y. Yiu and A. C. Yu, "Least-squares multi-angle doppler estimators for plane-wave vector flow imaging," *IEEE Trans. Ultrason., Ferroelectr., Freq. Control*, vol. 63, no. 11, pp. 1733–1744, 2016.

[7] J. Kortbek and J. A. Jensen, "Estimation of velocity vector angles using the directional cross-correlation method," *ieee transactions on ultrasonics, ferroelectrics, and frequency control*, vol. 53, no. 11, pp. 2036–2049, 2006.

[8] B.-F. Osmanski, M. Pernot, G. Montaldo, A. Bel, E. Messas, and M. Tanter, "Ultrafast doppler imaging of blood flow dynamics in the myocardium," *IEEE transactions on medical imaging*, vol. 31, no. 8, pp. 1661–1668, 2012.

[9] V. Perrot and D. Garcia, "Back to basics in ultrasound velocimetry: tracking speckles by using a standard piv algorithm," in *2018 IEEE International Ultrasonics Symposium (IUS)*. IEEE, 2018, pp. 206–212.

[10] E. Ecaterina, S. Stefania, C. Christoph, and J. Voorneveld, "A local spatio-temporal approach to plane wave ultrasound particle image velocimetry," 2017.

[11] B. E. Treeby and B. T. Cox, "k-wave: Matlab toolbox for the simulation and reconstruction of photoacoustic wave fields," *Journal of biomedical optics*, vol. 15, no. 2, p. 021314, 2010.

[12] J. A. Jensen, S. I. Nikolov, A. C. Yu, and D. Garcia, "Ultrasound vector flow imagingpart ii: Parallel systems," *IEEE Trans. Ultrason., Ferroelectr., Freq. Control*, vol. 63, no. 11, pp. 1722–1732, 2016.

[13] J. A. Tropp and A. C. Gilbert, "Signal recovery from random measurements via orthogonal matching pursuit," *IEEE Transactions on information theory*, vol. 53, no. 12, pp. 4655–4666, 2007.

[14] S. Chen and D. Donoho, "Basis pursuit," in *Proceedings of 1994 28th Asilomar Conference on Signals, Systems and Computers*, vol. 1. IEEE, 1994, pp. 41–44.

[15] D. Needell and R. Vershynin, "Signal recovery from incomplete and inaccurate measurements via regularized orthogonal matching pursuit," *IEEE Journal of selected topics in signal processing*, vol. 4, no. 2, pp. 310–316, 2010.

[16] M. M. Sejeso, "An l1-norm solution of under-determined linear algebraic systems using a hybrid method," Ph.D. dissertation, 2016.

[17] E. J. Candes, M. B. Wakin, and S. P. Boyd, "Enhancing sparsity by reweighted 1 minimization," *Journal of Fourier analysis and applications*, vol. 14, no. 5-6, pp. 877–905, 2008.

[18] D. Needell, J. Tropp, and R. Vershynin, "Greedy signal recovery review," in *2008 42nd Asilomar conference on signals, systems and computers*. IEEE, 2008, pp. 1048–1050.

[19] S. A. Razavi, E. Ollila, and V. Koivunen, "Robust greedy algorithms for compressed sensing," in *2012 Proceedings of the 20th European Signal Processing Conference (EUSIPCO)*. IEEE, 2012, pp. 969–973.

[20] D. Evans, "Colour flow and motion imaging," *Proceedings of the Institution of Mechanical Engineers, Part H: Journal of Engineering in Medicine*, vol. 224, no. 2, pp. 241–253, 2010.

[21] A. Swillens, P. Segers, H. Torp, and L. Lovstakken, "Two-dimensional blood velocity estimation with ultrasound: speckle tracking versus crossed-beam vector doppler based on flow simulations in a carotid bifurcation model," *IEEE transactions on ultrasonics, ferroelectrics, and frequency control*, vol. 57, no. 2, pp. 327–339, 2010.